Boundary-Layer Meteorol (2016) 158:383–408
DOI 10.1007/s10546-015-0097-6

ARTICLE

Linkages Between Boundary-Layer Structure and the Development of Nocturnal Low-Level Jets in Central Oklahoma

Petra M. Klein[1] · **Xiao-Ming Hu**[1] · **Alan Shapiro**[1] · **Ming Xue**[1]

Received: 27 May 2015 / Accepted: 6 October 2015 / Published online: 23 October 2015

Abstract In the Southern Great Plains, nocturnal low-level jets (LLJs) develop frequently after sunset and play an important role in the transport and dispersion of moisture and atmospheric pollutants. However, our knowledge regarding the LLJ evolution and its feedback on the structure of the nocturnal boundary layer (NBL) is still limited. In the present study, NBL characteristics and their interdependencies with LLJ evolution are investigated using datasets collected across the Oklahoma City metropolitan area during the Joint Urban field experiment in July 2003 and from three-dimensional simulations with the Weather Research and Forecasting (WRF) model. The strength of the LLJs and turbulent mixing in the NBL both increase with the geostrophic forcing. During nights with the strongest LLJs, turbulent mixing persisted after sunset in the NBL and a strong surface temperature inversion did not develop. However, the strongest increase in LLJ speed relative to the mixed-layer wind speed in the daytime convective boundary layer (CBL) occurred when the geostrophic forcing was relatively weak and thermally-induced turbulence in the CBL was strong. Under these conditions, turbulent mixing at night was typically much weaker and a strong surface-based inversion developed. Sensitivity tests with the WRF model confirm that weakening of turbulent mixing during the decay of the CBL in the early evening transition is critical for LLJ formation. The cessation of thermally-induced CBL turbulence during the early evening transition triggers an inertial oscillation, which contributes to the LLJ formation.

Keywords Low-level jet · Nocturnal boundary layer · Stable boundary layer

✉ Petra M. Klein
pkklein@ou.edu

Xiao-Ming Hu
xhu@ou.edu

1 School of Meteorology and Center for Analysis and Prediction of Storms, University of Oklahoma, 120 David L. Boren Blvd., Norman, OK 73072, USA

1 Introduction

While much progress has been made in understanding the daytime convective boundary layer (CBL) overland, our understanding regarding the nighttime boundary layer has progressed more slowly and many challenges remain (Banta et al. 2003, 2006, 2013; Mahrt 2007, 2009, 2011, 2014; Belusic and Guttler 2010; Fernando and Weil 2010; Lareau et al. 2013; Holtslag et al. 2013; Bosveld et al. 2014). Under clear skies, turbulence in the CBL is predominantly generated near the surface due to solar heating of the ground and is then transported upward throughout the CBL by updrafts and downdrafts that have turnover times on the order of tens of minutes and length scales of up to 2–3 km. In contrast, in the nocturnal boundary layer (NBL) an inversion layer forms near the surface under clear-sky conditions, in which thermal effects suppress the generation of turbulence by wind shear. Thus, turbulent mixing within the atmospheric boundary layer rapidly declines during the early evening transition, and may become weak and intermittent during very stable conditions (Acevedo and Fitzjarrald 2001; Mahrt 2010). The drastic decrease in turbulent mixing during the early evening transition is a key mechanism (Blackadar 1957; Shapiro and Fedorovich 2010) causing the formation of nocturnal low-level jets (LLJs). In the presence of LLJs, strong wind shear can sustain turbulent mixing and turbulence may be transported from aloft down to the surface (Smedman et al. 1997; Mahrt 1999; Ha and Mahrt 2001; Mahrt and Vickers 2002; Lundquist and Mirocha 2008; Hu et al. 2013b).

In the USA, LLJs are mostly documented and studied over the Great Plains (e.g., Bonner 1968; Mitchell et al. 1995; Stensrud 1996; Pan et al. 2004; Song et al. 2005; Jiang et al. 2007; Duarte et al. 2012; Pu and Dickinson 2014) and the eastern coastal area (Zhang et al. 2006; Helmis et al. 2013). The jet maximum (hereafter called the LLJ nose) typically develops at altitudes ranging from a few tens of metres to several hundreds of metres (Zhang et al. 2006; Cuxart and Jimenez 2007; Banta 2008; Werth et al. 2011; Wei et al. 2013). Several factors aid the formation of these nocturnal LLJs, including inertial oscillations (Blackadar 1957; Shapiro and Fedorovich 2010; Parish and Oolman 2010; Van de Wiel et al. 2010; Shibuya et al. 2014), baroclinicity generated by sloping terrain (Holton 1967), conservation of potential vorticity (Zhong et al. 1996), and large-scale meteorological forcing (Song et al. 2005; Wei et al. 2013; Hu et al. 2013b). However, the inertial oscillation theory appears incomplete as it cannot explain the geographical preference of LLJs and does not match well with observed LLJ characteristics (Lundquist 2003; Shapiro and Fedorovich 2009). The terrain-associated baroclinicity theory (Holton 1967) cannot correctly reproduce the jet-like vertical profiles (Shapiro and Fedorovich 2009). In the potential-vorticity conservation theory, northward-moving air becomes jet-like horizontally, as the Coriolis parameter increases with increasing latitude (Wexler 1961). However, this theory cannot explain the diurnal cycle of LLJs and their jet-like shape in the vertical. The development of LLJs may also be modulated by atmospheric radiative cooling (Holton 1967; Baas et al. 2009; Edwards et al. 2014) or, more generally, the surface energy balance (Fast and McCorcle 1990). Thus, the dynamical origin of nocturnal LLJs is still controversial and studies are still being conducted to extend/complete the previous theories (e.g., Shapiro and Fedorovich 2009; Van de Wiel et al. 2010).

Different theories regarding LLJ formation also have implications for vertical profiles of turbulence and other related meteorological and chemical variables (Kutsher et al. 2012). The time evolution and vertical distribution of mean and turbulent properties in the NBL are still active topics of research (Banta et al. 2006; Banta 2008; Karipot et al. 2008; Ohya et al. 2008; Chambers et al. 2011; Van de Wiel et al. 2012a; Hu et al. 2013a, d). Turbulent mixing in the NBL intensifies for wind speeds above a critical value (Sun et al. 2012; Bonin et al. 2015). For low wind speeds, the stable layer adjacent to the surface typically decouples from the residual layer, and the decay of mixing after the early evening transition produces sharp gradients in wind and temperature profiles near the surface. For higher wind speeds, stronger vertical mixing prevails near the surface and also between the surface and residual layer, i.e., these layers stay coupled (Acevedo et al. 2012; Hu et al. 2012). The impact of vertical mixing associated with LLJs on the vertical distribution of meteorological variables and chemical species needs to be further investigated (Banta et al. 2002; Cuxart and Jimenez 2007; Hu et al. 2012, 2013a, d; Williams et al. 2013).

In summary, open questions remain about LLJ evolution and LLJ interaction with the dynamic, thermodynamic, and turbulence structure of the NBL. In part, this is due to the lack of high-resolution profile measurements that range from the surface up to a few hundred metres above the LLJ nose (Conangla and Cuxart 2006; Pichugina and Banta 2010; Duarte et al. 2012; Deppe et al. 2013; Banta et al. 2013; Helmis et al. 2013; Mahrt et al. 2014; Wei et al. 2014; Klein et al. 2015). In the present study, linkages between characteristics of nocturnal LLJs and the structure of the atmospheric boundary layer before and after sunset are investigated. The analyses primarily use datasets collected during the Joint Urban field experiment in July 2003 (JU2003) in Oklahoma City. These datasets were selected as they provide detailed radar wind-profile measurements and turbulence quantities measured on an 80-m tower. Data from the Oklahoma Mesonet provide further information on near-surface winds and stability in the rural areas surrounding Oklahoma City, which were shown to be correlated with LLJ characteristics (Hu et al. 2013b). Previous analyses of the JU2003 datasets have demonstrated that LLJs occurred on approximately 85 % of the nights during the JU2003 study period (Lundquist and Mirocha 2008). Wang et al. (2007) concluded that the urban structures over downtown Oklahoma City lifted the LLJ nose by 25–100 m and reduced wind speeds below the LLJ nose by 10–15 %, but direct transport of turbulent momentum flux from the LLJ nose to the street level was not prominent. De Wekker et al. (2004) compared temperature and wind profiles measured 2 km upwind and 5 km downwind of the Oklahoma City central business district and found that above 200 m differences in wind speed were less than 0.5 m s^{-1} and in temperature less than 0.5°C both during day and night. Thus, urban effects did cause some changes in the LLJ characteristics but the urban impacts on the dynamics of the LLJ and its development are generally minor and less prominent than was observed in other cities (Kallistratova et al. 2009). Our previous studies using the JU2003 data focused on studying the differences in the thermodynamic and turbulence structure of the NBL for nights with both weak and strong LLJs and related impacts on the urban heat island intensity and nocturnal surface ozone concentrations (Hu et al. 2013b; Klein et al. 2014). The current study provides new insights into the scaling of the mean flow and turbulence in the NBL and the mechanisms leading to LLJ development. In addition to the JU2003 data analysis, three-dimensional simulations with the Weather Research and Forecasting (WRF) numerical model were conducted. Sensitivity tests with the WRF model reveal how the variation of turbulent friction affects LLJ development.

2 Method

2.1 Measurements

The JU2003 tracer experiment campaign took place in the Oklahoma City metropolitan area in July 2003 (Allwine 2004). During this experiment, a boundary-layer radar wind profiler was operated almost continuously during the month of July 2003 in Oklahoma City at the Argonne National Laboratory site, which was located 5 km downwind of the Oklahoma City

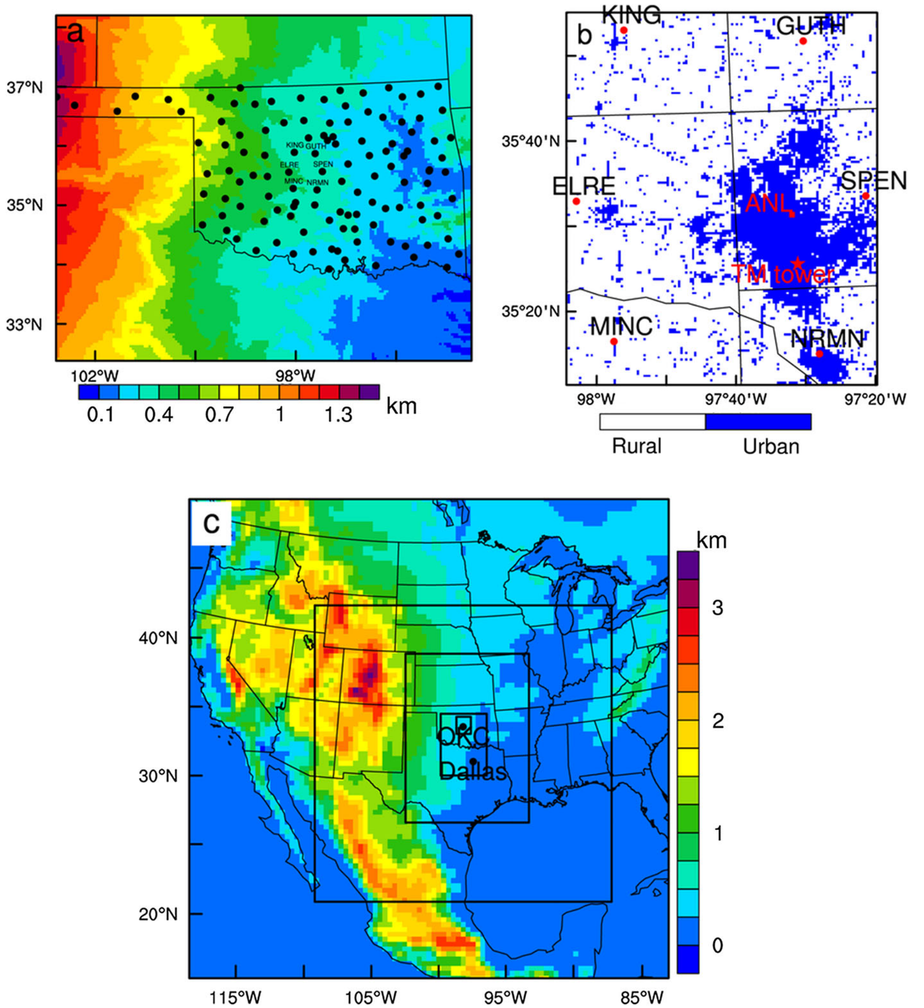

Fig. 1 **a** Map of Oklahoma with the locations of all Oklahoma Mesonet sites and **b** land-use categories (i.e., rural and urban) over the study area around Oklahoma City retrieved from the 2006 National Land Cover Data. The locations of six rural Mesonet sites around Oklahoma City (i.e., ELRE, GUTH, KING, MINC, NRMN, and SPEN) are marked by *dots*, the Argonne National Lab (ANL) site is marked by a *square*, and the Tyler Media (TM) tower is marked by a *star* on **b**. The *background colour* in **a** shows the terrain height in km. **c** Map of model domains and terrain heights (in km) used for the WRF model simulations

central business district in a suburban area (Fig. 1b). The wind profiler collected data with a vertical resolution of 55 m and an average time interval of 25 min, providing coverage from 82 m to approximately 2700 m above ground level (a.g.l.) (De Wekker et al. 2004).

Mean and turbulent flow properties were measured with sonic anemometers at 37.3 m and 79.6 m a.g.l. at the Tyler Media (TM) tower (Fig. 1b). The TM tower was located 5.5 km south of the Oklahoma City central business district in suburban terrain (Grimmond et al. 2004). The mean wind speeds measured at these levels, referred to as U_{37} and U_{80} thereafter, are used to evaluate the NBL shear near the surface and U_{37} is also used as a scaling velocity for turbulent quantities measured at the same height. Friction velocity u_*, defined as

$$u_* = \left[\left(\overline{u'w'} \right)^2 + \left(\overline{v'w'} \right)^2 \right]^{1/4}, \tag{1}$$

and the turbulent velocity scale U_t computed according to

$$U_\mathrm{t} = \sqrt{0.5 \left(\sigma_u^2 + \sigma_v^2 + \sigma_w^2 \right)} \tag{2}$$

are used to characterize the degree of turbulent mixing in the surface layer (see also Sun et al. 2012), with U_t^2 being a measure of the turbulence kinetic energy. The turbulent kinematic momentum fluxes $\overline{u'w'}$ and $\overline{v'w'}$ and standard deviations of the three velocity components σ_u, σ_v, σ_w, are computed using the sonic-anemometer data at the 37-m level. These data were originally processed using 30-min averaging periods, but for the current analysis the 30-min statistics are further averaged into hourly values.

Near-surface meteorological variables, including wind speed at 2 and 10 m a.g.l. and air temperature at 1.5 and 9 m a.g.l., routinely collected at the Oklahoma Mesonet sites, were also used in the analysis (McPherson et al. 2007). The mean spacing between Mesonet stations is approximately 30 km (Fiebrich and Crawford 2001). The average 10-m wind speed at the six Mesonet sites around Oklahoma City (Fig. 1a, b) is calculated and analysed as a measure of the near-surface wind field around Oklahoma City. To investigate the influence of atmospheric stability in the surface layer, the Richardson number (Ri) at the Mesonet sites is calculated as

$$Ri = \frac{g[(T_9 - T_{1.5})/\Delta Z_T + \Gamma_d]\Delta Z_u{}^2}{T_{1.5}[u_{10} - u_2]^2} \tag{3}$$

where g is the acceleration due to gravity, the dry adiabatic lapse rate $\Gamma_\mathrm{d} = 0.01\ \mathrm{K\ m^{-1}}$, T_9 and $T_{1.5}$ are the air temperatures measured at 9 and 1.5 m a.g.l., and u_2 and u_{10} are the wind speeds at 2 and 10 m a.g.l., respectively. The height differences between the measurement levels are $\Delta z_T = 7.5$ m for air temperature and $\Delta z_u = 8.0$ m for wind speed.

2.2 Numerical Simulations

To systematically investigate the relationship between LLJs and boundary-layer characteristics, numerical simulations with the WRF model, version 3.4.1 (Skamarock et al. 2008) were conducted for two contrasting episodes: strong LLJs during July 7–9, and weak LLJs during July 17–19. Simulations covering 42 h were initialized at 0000 UTC[1] on 7, 8, 17, and 18, July, respectively. The first 18 h of each simulation are treated as spin-up, and the remaining 24 h (from 1200 CST on day 1 to 1100 CST on day 2) are analysed. Five one-way nested domains (Fig. 1c) were employed, with horizontal grid spacings of 40.5, 13.5, 4.5, 1.5, and 0.5 km, respectively. This set-up was chosen because previous studies have shown that a 0.5-km grid spacing is needed to resolve urban effects on the boundary-layer structure over Oklahoma City (Liu et al. 2006; Lemonsu et al. 2009; Hu et al. 2013a, b, c, d). Each domain had 48 vertical layers extending from the surface to 100 hPa. The model sigma levels and mid-layer heights of the lowest 20 model layers are shown in Table 1. In all model domains, the Dudhia shortwave radiation algorithm (Dudhia 1989), the Rapid Radiative Transfer Model for longwave radiation (Mlawer et al. 1997), the WRF single-moment six-class (WSM6) microphysics scheme (Hong et al. 2004), and the Noah land-surface scheme coupled with a single-layer urban canopy model (Chen et al. 2011) were used. Our study focuses on days during which clouds and precipitation were absent over the study area. The microphysics

[1] UTC = Central Standard Time (CST) + 6 h.

Table 1 Sigma levels and mid-layer heights (m a.g.l.) of the lowest 20 model layers

Sigma levels	1.0	0.997	0.994	0.991	0.988	0.985	0.975	0.97	0.96	0.95
Mid-layer heights (m)	12	37	61	86	111	144	186	227	290	374
Sigma levels	0.94	0.93	0.92	0.91	0.895	0.88	0.865	0.85	0.825	0.8
Mid-layer heights (m)	459	545	631	717	826	958	1092	1226	1409	1640

The sigma levels are defined as $\frac{p-p_{\mathrm{top}}}{p_{\mathrm{surf}}-p_{\mathrm{top}}}$, where p is the dry hydrostatic pressure at each corresponding level, p_{surf} is dry hydrostatic surface pressure, and p_{top} is a constant dry hydrostatic pressure at model top

scheme is thus only of relevance for resolving cloud processes in the outer domains, which cover significant portions of North America and where clouds were present during the study period.

Planetary boundary-layer (PBL) schemes are used to parametrize turbulent vertical mixing of variables. The choice of PBL scheme affects the structure of the simulated boundary layers and the predicted vertical mixing, which leads to differences in the predicted LLJ strength (Storm et al. 2009; Nielsen-Gammon et al. 2010; Shin and Hong 2011; Hu et al. 2013a; Draxl et al. 2014). In order to investigate the impact of the boundary-layer characteristics on LLJ formation, a sensitivity analysis is conducted for the Yonsei University (YSU, Hong et al. 2006; Hong 2010) PBL scheme. The YSU scheme is a first-order non-local scheme, with a counter-gradient term and an explicit entrainment term in the turbulence diffusion equation, which was shown to reproduce important features of the NBL (Hu et al. 2013a, c). In the YSU PBL scheme, the eddy viscosity for the stable boundary layer is formulated as

$$K_{\mathrm{m}} = k w_{\mathrm{s}} z \left(1 - \frac{z}{h}\right)^2, \tag{4}$$

where the velocity scale is $w_{\mathrm{s}} = u_*/\phi_{\mathrm{m}}$, k is the von Karman constant, z is the height above ground, and h is the boundary-layer height diagnosed in the YSU scheme using a critical Richardson number (0.25 over the land, while it depends on surface winds and Rossby number over oceans). The non-dimensional profile function, ϕ_m, for stable conditions ($z/L > 0$) in YSU is implemented as

$$\phi_{\mathrm{m}} = 1 + a\left(\frac{z}{L}\right), \tag{5}$$

where L is the Obukhov length. The coefficient a, which describes the dependence of eddy viscosity on the stability parameter (z/L), plays an important role for simulating LLJs. Its default value in YSU is 5 (Nielsen-Gammon et al. 2010; Hu et al. 2013a). Sensitivity simulations with a varying between 0.1 and 10 were conducted, noting that the lower and higher values of this range may exceed the plausible range of a to accurately simulate the realistic vertical mixing in NBL (Foken 2006; Nielsen-Gammon et al. 2010). These extreme, somewhat unrealistic, values were included to emphasize the role of stability and vertical mixing in LLJ development. For the conducted sensitivity simulations, only the eddy conductivity

$$K_{\mathrm{h}} = Pr^{-1} K_{\mathrm{m}}, \tag{6}$$

where Pr is the turbulent Prandtl number, was available in the WRF model output. We thus used K_{h} to characterize the diurnal evolution of vertical turbulent mixing in the boundary layer, but verified for the control simulation (with $a = 5$) that the profiles for eddy viscosity and conductivity are similar.

3 Results

3.1 Observed LLJ Properties

During July 2003, southerly winds dominated and LLJs developed in Oklahoma on a majority of the nights (Fig. 2a, b). Notable exceptions were July 1, when an easterly wind persisted due to a tropical depression east of Oklahoma, and July 22–23, 29–30, and July 10, when northerly winds dominated due to cold frontal passages. On one to two nights after each cold frontal passage, the LLJs were typically relatively weak. In July 2003, the LLJ nose was usually at about 400 m and never above 800 m (Figs. 2a, 3). Following Hu et al. (2013b), the maximum jet speed, U_{LLJ}, was thus determined as the hourly maximum wind speed observed in the layer between 200 and 800 m. The lower limit of 200 m was chosen, as the radar wind-profile data may not be accurate below these heights.

The Richardson number Ri (Eq. 3) shows distinct diurnal patterns around Oklahoma City during the study period (Fig. 2c). It increases prominently during the early evening transition and remains positive until the next morning when the rapidly developing CBL breaks down the near-surface inversion. As, the day-to-day variation of Ri is prominent, one objective of our study is to investigate the relationships between atmospheric stability and LLJ strength. We selected a 12-h time period for each day/night ranging from 1730 to 0430 local time (LT, the same as CDT). The analyzed data were limited to days/nights for which the wind directions measured at the TM tower at 37 and 80-m a.g.l. were within a southerly sector (135°–225°), and for which the observations had no major gaps during the selected 12-h

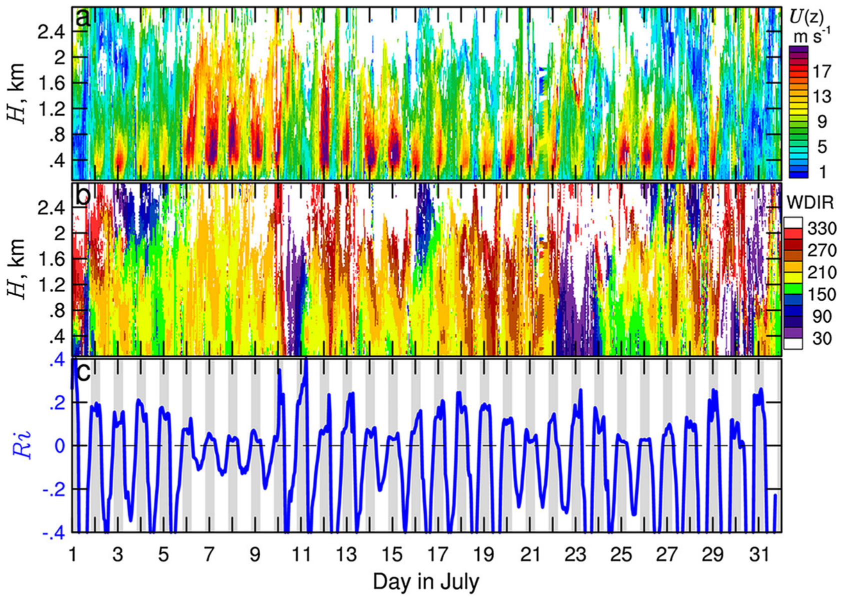

Fig. 2 Time-height diagram of **a** wind speed and **b** wind direction in July 2003 at the ANL site observed with a boundary-layer radar wind profiler, and **c** time series of Richardson number (Ri) averaged over six Oklahoma Mesonet sites. Periods of sunset to sunrise (i.e., 1942–0527 CST) are *shaded* in the *middle panel*. Note the heights in panels **a** and **c** are above ground level and the daytime values of *Ri* on some days are lower than −0.4, but this lower limit was chosen to better document the *Ri* values during the early evening transition and at night

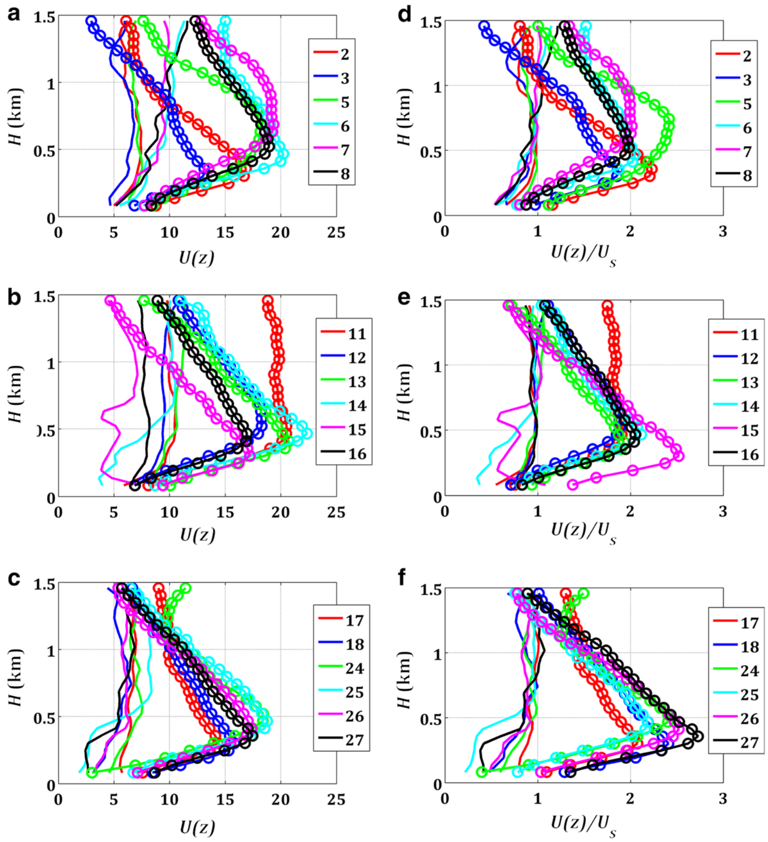

Fig. 3 **a**–**c** Observed averaged daytime and nighttime wind profiles for the 18 days included in the analysis and **d**–**f** corresponding normalized profiles whereby the wind speed at 800 m above ground from the daytime profile is used as scaling velocity U_{s} for both daytime (*solid lines*) and nighttime (*solid lines* and *circles*) profiles. The *vertical axis* refers to the height H a.g.l in km. See text for more details

windows. The time period was chosen for the transition from the afternoon CBL to the stable NBL. The sunset times, which ranged from 2049 to 2035 LT in July 2003, were taken into account when defining the time window. Table 2 lists the 18 days in July 2003 included in the analysis and provides an overview of important boundary-layer parameters, which are defined and discussed below. Each listed date refers to the day at the beginning of the time window. The sonic anemometer at the 37-m level became fully operational only on July 6, which is why data are missing for the first three days. Daytime and nighttime wind profiles for the selected nights are shown in Fig. 3a–c. The daytime profile was computed as the average of the 1730 and 1830 LT observations, for the nighttime profile three hourly profiles from 0130 to 0330 LT were averaged since the properties of the LLJ for most days did not vary much in that time period. The profiles show that the daytime values of U_{LLJ}, computed as the maximum wind speed below 800 m, are representative of the mixed-layer wind speeds in the daytime CBL while at night U_{LLJ} corresponds to the LLJ wind-speed maximum.

The daily time series of the wind speeds U_{LLJ}, U_{37}, and U_{80}, friction velocity u_*, turbulent velocity scale U_{t}, and Richardson number Ri for the 18 selected days are shown in Fig. 4. The transition from unstable conditions ($Ri < 0$) to stable conditions ($Ri > 0$) occurs at around

Table 2 Summary of LLJ, near-surface stability, and turbulence parameters observed during the study period

Day	$(U_{\mathrm{LLJ}})_{\max}$ (m s^{-1})	U_{s} (m s^{-1})	$(U_{\mathrm{LLJ}}/U_{\mathrm{s}})_{\max}$	$(U_{\mathrm{LLJ}}/U_{37})_{\max}$	$(U_{80}/U_{37})_{\max}$	Ri_{night}	Ri_{day}	$U_{\mathrm{t,night}}$ (m s^{-1})	$U_{\mathrm{t,day}}$ (m s^{-1})	$(U_{\mathrm{t}}/U_{37})_{\mathrm{night}}$	$(U_{\mathrm{t}}/U_{37})_{\mathrm{day}}$
2	17.2	7.6	2.3	N/A	N/A	0.12	−0.22	N/A	N/A	N/A	N/A
3	14.4	7.8	1.8	N/A	N/A	0.21	−0.17	N/A	N/A	N/A	N/A
5	19.4	8.0	2.4	3.6	1.3	0.08	−0.18	1.0	N/A	0.20	N/A
6	21.7	9.8	2.2	3.9	1.3	0.06	−0.07	1.0	1.7	0.18	0.23
7	21.1	9.9	2.1	3.4	1.4	0.04	−0.12	1.0	1.5	0.19	0.21
8	20.5	9.8	2.1	3.5	1.3	0.07	−0.08	1.1	1.5	0.19	0.21
11	21.0	10.8	2.0	3.5	1.4	0.09	−0.09	1.0	1.6	0.16	0.23
12	19.5	9.8	2.0	3.6	1.4	0.24	−0.26	0.9	1.5	0.17	0.28
13	20.8	10.9	1.9	3.5	1.4	0.07	−0.14	1.1	1.4	0.18	0.22
14	22.5	10.9	2.1	3.2	1.3	0.04	−0.10	1.4	1.6	0.18	0.23
15	17.6	6.8	2.6	3.0	1.4	0.15	−0.21	1.0	1.4	0.18	0.21
16	17.6	8.4	2.1	4.1	1.6	0.18	−0.24	0.7	1.3	0.16	0.25
17	15.1	6.9	2.2	3.6	1.7	0.25	−0.27	0.5	1.3	0.13	0.25
18	16.2	6.6	2.5	4.4	1.7	0.19	−0.37	0.4	1.2	0.12	0.36
24	18.7	7.7	2.4	3.1	1.4	0.04	−0.25	1.0	1.5	0.18	0.24
25	19.0	8.7	2.2	3.2	1.4	0.03	−0.20	1.2	1.5	0.18	0.21
26	18.4	6.9	2.7	3.2	1.3	0.10	−0.37	1.0	1.5	0.18	0.30
27	17.8	6.5	2.7	3.6	1.5	0.11	−0.38	0.8	1.4	0.16	0.30
Max	22. 5	10.9	2. 7	4.4	1.7	0.25	−0.07	1.4	1.7	0.20	0.36
Min	14.4	6.5	1.8	3.0	1.3	0.03	−0.38	0.4	1.2	0. 12	0.21

See text for details of definitions of the parameters. The numbers in the first column refer to the day in July 2003

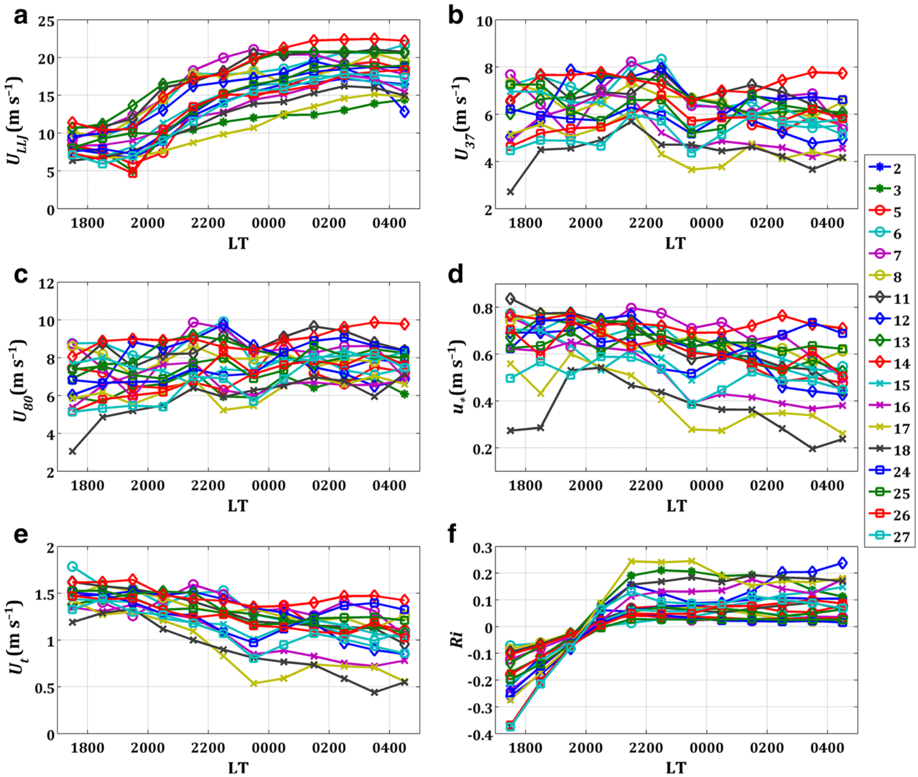

Fig. 4 Temporal evolution of **a** LLJ strength U_{LLJ}, **b**–**c** wind speeds measured with sonic anemometers at the TM tower at 37 m (U_{37}) and 80 m (U_{80}) above ground, **d**–**e** friction velocity u_* and turbulent velocity scale U_{t}, both also measured with the 37-m sonic anemometer, and **f** stability parameter *Ri* computed from wind and temperature data at six rural Mesonet sites using Eq. 3. All wind speeds are plotted in m s^{-1} and the legend refers to the day in July 2003

2000 LT (Fig. 3f). Around that time, U_{LLJ} begins to increase until levelling off at around 0100 on most nights. On seven days, U_{LLJ} decreases at around 1930 LT (most pronounced on July 3 and July 26) before the flow starts to accelerate. Recently, Van de Wiel et al. (2010) discuss that backward inertial oscillations can initially cause a decrease in wind speed but such backward oscillations should occur below a crossing point near the surface. Here, we focused on analyzing correlations between bulk LLJ and turbulence characteristics and did not further investigate whether backward oscillations caused the observed initial decreases in wind speed.

During the 18 nights analysed, the maximum LLJ speed $(U_{\mathrm{LLJ}})_{\mathrm{max}}$ observed each night varied between 14.4 and 22.5 m s^{-1} (Table 2) while the shape of the daily time series of U_{LLJ} is quite similar (Fig. 4). Following the inertial oscillation theory, the LLJ speed depends on the deviation of boundary-layer winds from the geostrophic wind, i.e., the ageostrophic wind speed (Shapiro and Fedorovich 2010; Van de Wiel et al. 2010). Obtaining reliable estimates of the geostrophic wind speed proved to be challenging, i.e., we could not compute the ageostrophic wind speed that has been proposed as a scaling velocity (e.g., Shapiro and Fedorovich 2010; Van de Wiel et al. 2010). Above 800 m, the daytime wind-speed profiles (average of the profiles measured at 1730–1830 LT) show little variability, i.e., the daytime values of U_{LLJ} are a good approximation of the mixed-layer wind speed in the CBL (Fig. 3a–c). Thus, we decided to define the daytime values of U_{LLJ}, as a scaling velocity U_s. While we expect the geostrophic wind speed to be higher than U_s, we hypothesize that this scaling velocity serves as a proxy, allowing us to account for the variability in the geostrophic forcing. The values of U_s ranged from 6.5 to 10.9 m s^{-1} during the study period (Table 2). Normalized daytime and nighttime profiles using U_s as scaling velocity are shown in Fig. 3d–f. It can be noted that days with the highest velocity increase at night, i.e., days with the highest U_{LLJ}/U_s values, are not days with the highest values of U_{LLJ}. While the normalized profiles show less variability than the original wind profiles, the relative LLJ strength and height still vary from day to day. Finding the factors causing this variability is an important objective of this study.

The trends in the time series of U_{37}, and U_{80} are less consistent (Fig. 4b, c) than the trends in U_{LLJ}, and also the friction velocities u_* vary strongly (Fig. 4d) whereby large differences are particularly noticeable before sunset: on some days a pronounced increase in u_* is observed before the early evening transition while on other days a gradual decline or high variability from hour to hour can be noted. The turbulent velocity scale U_t, on the other hand, shows similar trends for all days and more consistent trends throughout the selected 12-h time window. Thus, U_t is used as a parameter to quantify the level of turbulent mixing in the NBL, which is also consistent with Sun et al. (2012). The Ri profiles have similar shapes but both the afternoon values Ri_{day} (minimum Ri value before sunset) and nighttime value Ri_{night} (maximum Ri value observed between 2230 and 0430 LT) vary daily during the study period (Fig. 3f). The values Ri_{night} ranged from 0.03 to 0.25, i.e., from quasi-neutral to moderately stable conditions, while Ri_{day} values in the range -0.07 to -0.38 were observed (Table 2).

As discussed in Shapiro and Fedorovich (2010) and Van de Wiel et al. (2010), the LLJ starts to develop as an inertial oscillation from the initial afternoon wind profile and the increase in wind speed relative to the initial wind speed is an important parameter that describes the LLJ strength. In our analysis, the wind-speed ratio U_{LLJ}/U_s describes the increase of the wind speed at the LLJ nose relative to the initial mixed-layer wind speed. The diurnal time series of U_{LLJ}/U_s (Fig. 5a) show the expected sharp increase of U_{LLJ}/U_s after the early evening transition. The variation of U_{LLJ}/U_s with Ri further highlights the sharp increase as stability changes from unstable to stable conditions. However, the U_{LLJ}/U_s values start to decline again for $Ri > 0.1$ and a clear correlation between Ri at night ($Ri > 0.1$) and U_{LLJ}/U_s does not emerge (Fig. 5d). The daily maximum values of $(U_{LLJ}/U_s)_{max}$ ranged between 1.8 and 2.7 (Table 2). As additional parameters describing the dynamic and turbulent structure of the NBL, the velocity ratio U_{80}/U_{37}, and turbulent velocity scale U_t/U_{37} normalized by the wind speed measured at the same height and time are also plotted in Fig. 5. The ratio U_{80}/U_{37} can serve as a dimensionless shear parameter, since

$$\frac{U_{80}}{U_{37}} = \left(\frac{80-37}{U_{37}}\right)\frac{\mathrm{d}U}{\mathrm{d}z} + 1, \tag{7}$$

which describes the degree of shear below the LLJ nose. The ratio U_t/U_{37} is a measure of the turbulence intensity. The variation of U_t/U_{37} with stability is more consistent than for U_{LLJ}/U_s: turbulence intensity decreases nearly linearly as Ri increases (Fig. 5f). Similar to U_{LLJ}/U_s, the shear parameter U_{80}/U_{37} increases drastically after Ri becomes positive, but a clear correlation between Ri and U_{80}/U_{37} does not emerge (Fig. 5f). It is interesting to note that high values of $(U_{LLJ}/U_s)_{max}$, i.e., the development of a strong LLJ relative to the previous day mixed-layer wind speed, appear to be more prominent on days with lower Ri_{day} values, such as e.g., on July 18, 26, and 27 (Table 2; Fig. 5d). During these three days, the highest turbulence intensities U_t/U_{37} (Fig. 5b, e) were observed in the CBL. The correlation

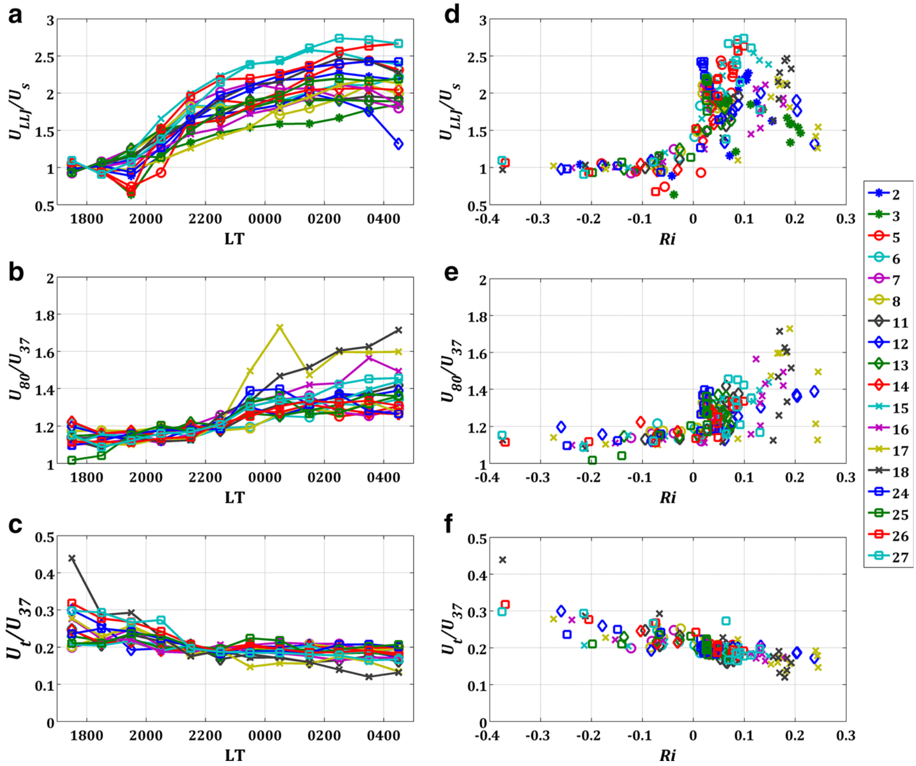

Fig. 5 Temporal evolution of **a** relative LLJ strength $U_{\mathrm{LLJ}}/U_{\mathrm{s}}$, **b** wind-speed ratio U_{37}/U_{80} that serves as shear parameter, and **c** turbulence intensity U_{t}/U_{37}. Panels **d**–**f** show the same three parameters but plotted as a function of the stability parameter *Ri* instead of as a function of time. The legend refers to the day in July 2003

of relative LLJ strength $(U_{\mathrm{LLJ}}/U_{\mathrm{s}})_{\mathrm{max}}$ with atmospheric stability *Ri* and turbulence intensity U_{t}/U_{37} is now investigated in more detail.

Following the inertial oscillation theory, the decrease in turbulent vertical mixing during the early evening transition determines the strength of the LLJ relative to the initial (afternoon mixed-layer) wind speeds (Shapiro and Fedorovich 2010; Van de Wiel et al. 2010). Thus, we propose the hypothesis that the highest increase of the LLJ speed relative to the initial mixed-layer wind speed, i.e., the highest value of $(U_{\mathrm{LLJ}}/U_{\mathrm{s}})_{\mathrm{max}}$, is expected during nights with, (i) the largest change in atmospheric stability, i.e., largest values of $Ri_{\mathrm{night}} - Ri_{\mathrm{day}}$, and (ii) the largest decrease in turbulence intensity U_{t}/U_{37} during the early evening transition. During the study period, the change in atmospheric stability, $Ri_{\mathrm{night}} - Ri_{\mathrm{day}}$, varied from 0.13 on July 6 to 0.57 on July 18. To assess the change in turbulence intensity, we computed a daytime value $(U_{\mathrm{t}}/U_{37})_{\mathrm{day}}$ as a mean value for the time period 1730-1830 LT, and nighttime value $(U_{\mathrm{t}}/U_{37})_{\mathrm{night}}$ as the minimum value observed between 2230 and 0430 LT (Table 2). During the study period, the ratio $(U_{\mathrm{t}}/U_{37})_{\mathrm{night}}$ / $(U_{\mathrm{t}}/U_{37})_{\mathrm{day}}$, which describes the decrease in turbulence intensity in the NBL relative to the CBL, ranged between 0.33 on July 18 and 0.91 on July 7.

Plots of relative LLJ strength $(U_{\mathrm{LLJ}}/U_{\mathrm{s}})_{\mathrm{max}}$ versus change in stability $Ri_{\mathrm{night}} - Ri_{\mathrm{day}}$ (Fig. 6a), and turbulence-intensity ratio $(U_{\mathrm{t}}/U_{37})_{\mathrm{night}}$ / $(U_{\mathrm{t}}/U_{37})_{\mathrm{day}}$ (Fig. 6d) show the

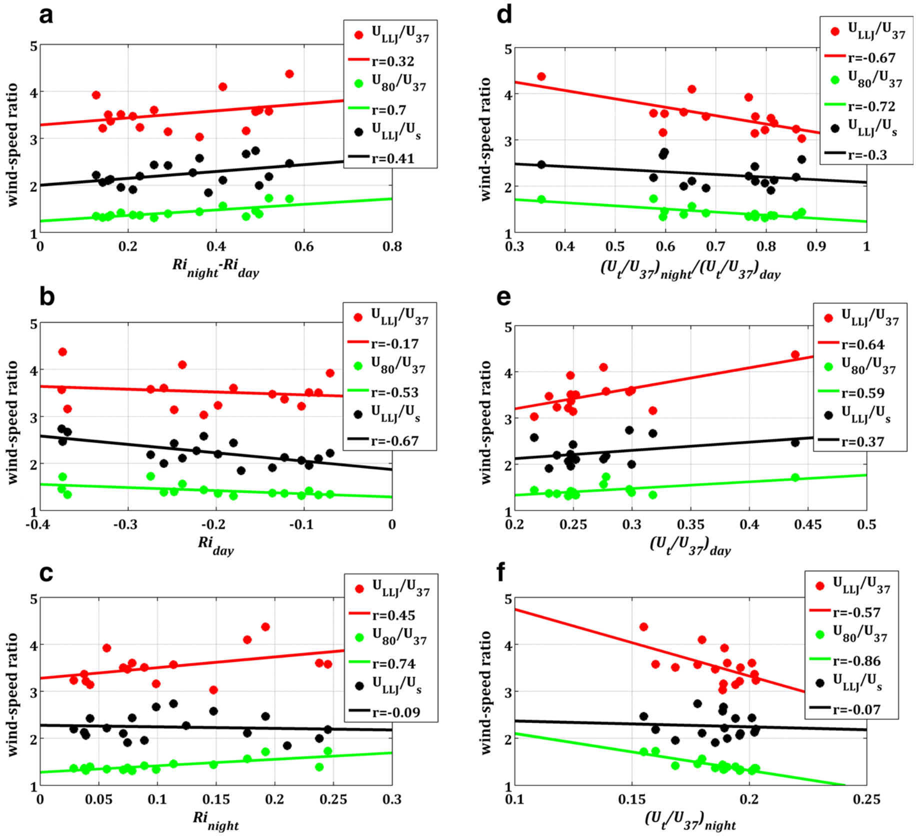

Fig. 6 Plots of relative LLJ strength U_{LLJ}/U_s and shear parameters U_{37}/U_{80} and U_{LLJ}/U_{80} versus **a** night-to-day change in stability Ri_{night} - Ri_{day}, **b** daytime stability Ri_{day}, **c** nighttime stability Ri_{night}, **d** night-to-day change in turbulence intensity $(U_t/U_{37})_{night}$ / $(U_t/U_{37})_{day}$, **e** daytime turbulence intensity $(U_t/U_{37})_{day}$, and **f** nighttime turbulence intensity $(U_t/U_{37})_{night}$. See text for more details

expected trends: $(U_{LLJ}/U_s)_{max}$ increases as $Ri_{night} - Ri_{day}$ increases and as $(U_t/U_{37})_{night}$ / $(U_t/U_{37})_{day}$ decreases. The scatter in the data is however fairly large and the correlation coefficients r are quite low (0.41 and 0.3 respectively). In addition to relative LLJ strength, the shear parameters U_{80}/U_{37} and U_{LLJ}/U_{37} are also plotted in Fig. 6. As one would expect, both shear parameters also increase with increasing $Ri_{night} - Ri_{day}$ and decrease with increasing $(U_t/U_{37})_{night}$ / $(U_t/U_{37})_{day}$. The corresponding correlation coefficients are quite high, particularly for U_{80}/U_{37} and $(U_t/U_{37})_{night}$ / $(U_t/U_{37})_{day}$, as in that case all variables were measured at the same site and with the same instruments.

As mentioned above, the relative LLJ strength $(U_{LLJ}/U_s)_{max}$ tended to be higher on days with lower Ri values (characterizing stronger convective turbulence) before the early evening transition. We thus also investigated correlations of the relative LLJ strength and shear parameters with values of daytime and nighttime stability (Ri_{day} and Ri_{night}) and turbulence intensity ($(U_t/U_{37})_{day}$ and $(U_t/U_{37})_{night}$). Of all six parameters represented in Fig. 6, relative LLJ strength $(U_{LLJ}/U_s)_{max}$ correlates best with Ri_{day} (Fig. 6b) and shows no correlation with Ri_{night} (Fig. 6c) or $(U_t/U_{37})_{night}$ (Fig. 6f). Shear parameters, on the other hand, are best correlated with $(U_{\mathrm{t}}/U_{37})_{\mathrm{night}}$ (Fig. 6f). Thus, in our study, relative LLJ strength primarily depends on daytime stability and turbulence intensity but is not noticeably affected by nighttime stability. One interpretation concerns the collapse of the CBL during the early evening transition being the main mechanism for initial LLJ development. The LLJ then persists throughout the night with its bulk characteristics not being much affected by nighttime stability and turbulence intensity. The latter two parameters do however modulate the shear below the LLJ nose. At the same time, nighttime stability and turbulence parameters are also modulated by the presence of the LLJ at night. As a consequence, the values of $(U_{\mathrm{t}}/U_{37})_{\mathrm{night}}$ do not vary much throughout the study period, i.e., daily variations in the turbulence intensity ratios $(U_{\mathrm{t}}/U_{37})_{\mathrm{night}}\,/\,(U_{\mathrm{t}}/U_{37})_{\mathrm{day}}$ are primarily due to variations in the daytime values. Our findings overall confirm the hypotheses that were formulated above based on the inertial oscillation theory: the relative LLJ strength depends on the degree of change in atmospheric stability and turbulence intensity during the early evening transition. Additionally, we have shown that the conditions in the daytime CBL just before sunset are critical and Ri_{day} is a good indicator of the strength of LLJ. These conclusions may not be applicable to situations with weaker jets and a strongly stable NBL.

So far, the analysis follows the concepts outlined in Shapiro and Fedorovich (2010) and Van de Wiel et al. (2010) and our conclusions are based on relative LLJ strength, i.e., the increase in velocity relative to the mixed-layer velocity prior to the early evening transition. We would like to point out that such normalization by an initial wind speed is critical. As shown in Fig. 7, very different conclusions could be drawn if the absolute wind speed U_{LLJ} is plotted against atmospheric stability. The daily maximum values of U_{LLJ} correlate well with all three stability parameters $Ri_{\mathrm{night}} - Ri_{\mathrm{day}}$, Ri_{night}, and Ri_{day} but the LLJ strength increases as the absolute values of Ri decrease, i.e., when the flow becomes more neutral. One may thus conclude that stability effects play no important role in LLJ development and that the LLJ weakens as the daytime CBL becomes more unstable and the NBL more stable. However, the fact that stronger LLJs correspond with more neutral conditions merely reflects that atmospheric stability, in general, decreases as wind speed increases. As illustrated in Fig. 7, the same trends are observed for the average wind speeds measured 10 m above ground (U_{10}) at the six rural Mesonet sites and for the wind speeds measured at the TM tower (U_{37} and U_{80}). Appropriate normalization of the data is thus key for understanding which factors play a role in the development and evolution of LLJs. In our study, using the daytime mixed-layer wind speed as a scaling velocity U_{s} allows us to account for the general trends in the geostrophic forcing and to analyze the data in a non-dimensional framework.

Similarly, we point out the importance of using turbulence intensities U_{t}/U_{37} rather than original values of U_{t} when investigating the role of turbulent mixing in LLJ development. There are no big differences in the nighttime to daytime ratios of these two quantities (Figs. 6d, 7d), but opposite trends are observed in the correlation of $(U_{\mathrm{LLJ}}/U_{\mathrm{s}})_{\mathrm{max}}$ with daytime values: while we observe the expected trend of stronger daytime turbulence intensities $(U_{\mathrm{t}}/U_{37})_{\mathrm{day}}$ promoting stronger LLJs, higher absolute values of $U_{\mathrm{t,day}}$ correlate with weaker LLJs. One explanation is that the decline in turbulent mixing during the early evening transition, which drives the inertial oscillation, is primarily due to the shut down of thermally-driven turbulence when the CBL collapses. High values of $U_{\mathrm{t,day}}$ can be observed during days with high wind speeds during which thermally-driven turbulent mixing is of secondary importance. Thus, the magnitude of $U_{\mathrm{t,day}}$ does not correlate well with the level of thermally-driven turbulence and is inadequate as parameter for LLJ development. On the other hand, turbulence intensities describe the strength of

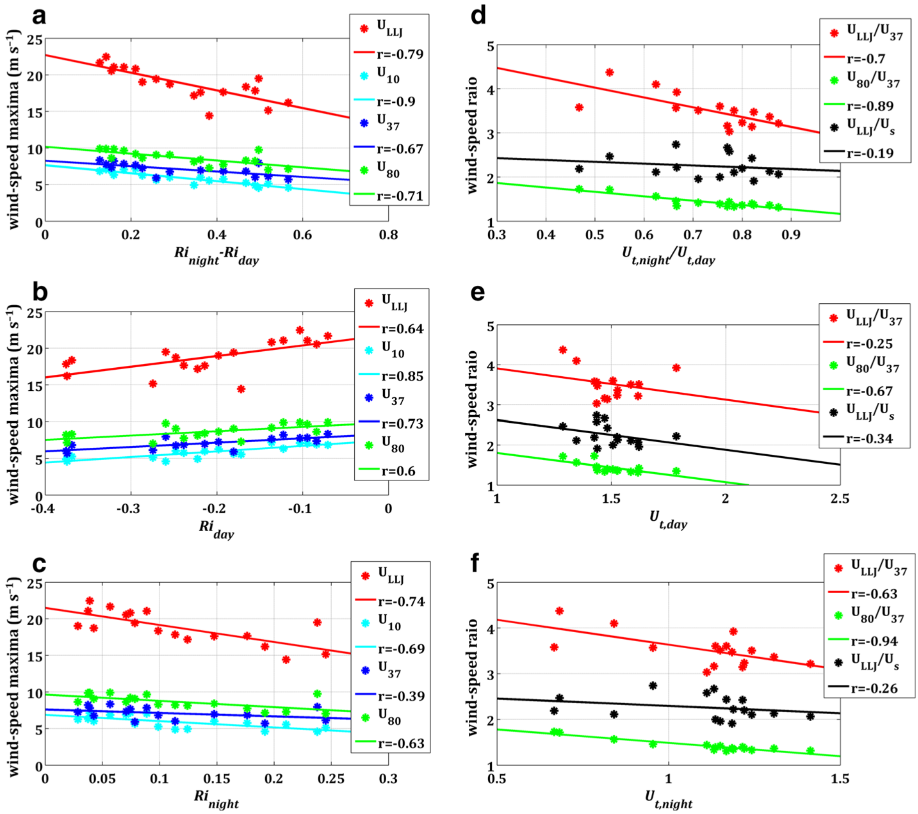

Fig. 7 Similar to Fig. 6, but instead of normalized velocities absolute velocities are plotted against **a** night-to-day change in stability Ri_{night}- Ri_{day}, **b** daytime stability Ri_{day}, **c** nighttime stability Ri_{night}. In panels **d**–**f**, the normalized velocities are plotted against turbulent velocity scales instead of turbulence intensities. See text for more details

turbulent mixing relative to the mean flow and are better indicators of thermally-driven turbulence.

3.2 Analysis of Selected Episodes

The interdependence between boundary-layer characteristics/structures and LLJs are further examined in detail for two contrasting episodes during July 7–9 and during July 17–19 (Fig. 8). The maximum LLJ wind speeds exceeded 21 m s^{-1} during the July 7–9 episode, while they stayed around 15 m s^{-1}during the July 17–19 episode (Table 2; Fig. 4), i.e., in terms of absolute wind speeds, a weaker LLJ developed during the second episode. However, the strongest increase relative to the daytime wind speeds was observed during the night of July 18–19. On July 18, daytime stability Ri_{day} was -0.37, while the CBL during the first episode was less unstable ($Ri_{\text{day}} \approx -0.1$). Of all the days analyzed, daytime turbulence intensity, $(U_t/U_{37})_{\text{day}}$, was highest on July 18, which further indicates that the contribution of thermally-driven turbulent mixing in the CBL was stronger during the second than the first episode. Synoptic flow patterns played an important role in modulating the wind speeds for the two episodes. During July 7–9, the pressure gradient over most of the Great Plains

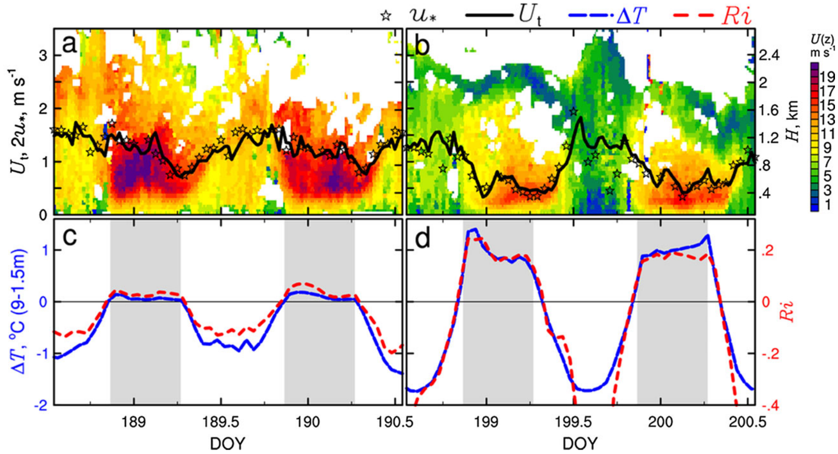

Fig. 8 **a**, **b** Time–height diagram of horizontal wind speed observed by the boundary-layer wind profiler overlaid with the time series of turbulent velocity scale U_t and frictional velocity u_* and **c**, **d** time series of mean inversion strength (ΔT between 1.5 and 9 m) and Ri at the six mesonet sites during the periods of (*left*) July 7–9 (DOY 188–190) and (*right*) July 17–19, 2003 (DOY 198–200). Periods of sunset to sunrise are *shaded* in the *bottom panel*

was north-west to south-east. Such a synoptic-scale weather pattern predominates during the warm season (Song et al. 2005). The horizontal pressure gradient and the blocking effect of the Rockies (see terrain height in Fig. 1c) forced airflow from southerly latitudes into the south-central United States, thus contributing to strong southerly or south-westerly winds during the nighttime (Figs. 2b, 8a). During July 17–19, the pressure gradient was weak in Oklahoma, resulting in weaker prevailing southerly to south-westerly winds (Figs. 2b, 8b).

Weaker/stronger winds are associated with weaker/stronger turbulence near the surface during the nighttime (Fig. 8a, b). During the July 17–19 episode, turbulence subsided quickly during the early evening transitions as indicated by a sharp decrease of the turbulent velocity scale U_t and friction velocity u_*. As discussed above, the nighttime turbulence intensities decreased to approximately 30 % of the daytime values on July 18. In contrast, the turbulent velocity scale U_t remained relatively high throughout the nights of July 7–9 and on July 7 the nighttime turbulence intensity was still approximately equal to 90 % of the corresponding daytime value (Table 2). The sharper decrease in turbulence intensity during the second episode was associated with higher values of $(U_{LLJ}/U_s)_{max}$ than during the first episode. Differences in the nighttime turbulence intensities also were associated with clear differences in nighttime stability: higher wind speeds and higher turbulence intensities at night were associated with stronger coupling in the layer below the LLJ nose as indicated by the smaller values of the shear parameter $(U_{80}/U_{37})_{max}$ (Table 2; Fig. 5b) and lower Ri_{night} values (Fig. 8c) during the first episode, while nighttime wind shear (Fig. 5b) and stability quickly increased (Fig. 8d) due to surface radiative cooling in the absence of strong turbulence during the second episode. Differences can also be noted in the heights of the LLJ nose: during the second episodes the LLJ was lower than during the first episode. Our finding of nighttime turbulence increasing with large-scale pressure gradient forcing is consistent with Van de Wiel et al. (2012b), who found that nighttime near-surface turbulence increased rapidly when the geostrophic wind speed exceeded 5 m s^{-1}.

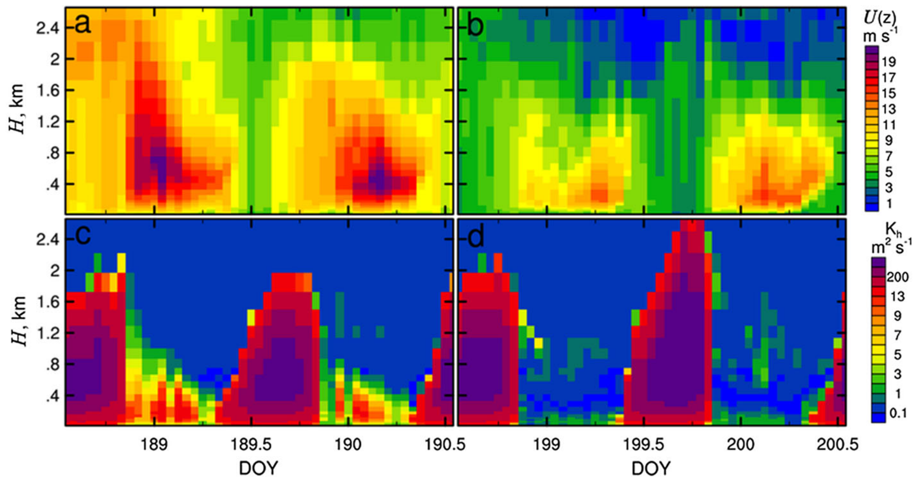

Fig. 9 Time–height diagram of **a**, **b** horizontal wind speed $U(z)$ and **c**, **d** eddy conductivity K_h during the periods of (*left*) July 7–9 (DOY 188–190) and (right) July 17–19, 2003 (DOY 198–200) simulated with the WRF model using the default YSU PBL scheme (i.e., $a = 5$)

3.3 Simulations with the WRF Model for the Selected Episodes

To further investigate the linkages of LLJ development and NBL structure, sensitivity studies were conducted with the WRF model in which the stability dependence of the eddy diffusivities for heat and momentum was systematically varied. The control simulations with default WRF model parameters successfully capture the differences in LLJ strength between the two episodes (Fig. 9a, b). On each day, turbulent vertical mixing (as characterized by the eddy conductivity K_h) in the boundary layer shows a prominent diurnal variation (Fig. 9c, d). Vertical mixing clearly weakens drastically after sunset. However, while it becomes nearly negligible in the residual layer, some mixing persists in the stable boundary layer throughout the night (Fig. 9c, d).

The results from the WRF model sensitivity tests with different values for the coefficient a in the stability functions ϕ_m (Eq. 5) used in the YSU PBL scheme illustrate the feedback of boundary-layer characteristics on LLJ development. In all simulations, the LLJ nose occurs near the top of the stable boundary layer (i.e., near the transition to the residual layer), where vertical mixing sharply declines (Fig. 10a, b) and the flow becomes effectively inviscid. Weak vertical mixing confined in a shallower stable boundary layer leads to lower LLJs (Fig. 10a–d). This is consistent with the observational study of Pichugina and Banta (2010), which reports that for a LLJ with a distinct nose, the height of the LLJ nose is approximately the height of the first significant minimum in the turbulence profile (or top of the stable boundary layer). Sharp contrasts in simulated nighttime stability during the two episodes also exist, which further documents how vertical mixing modulates boundary-layer stability (Fig. 11e, f). During episode 1, when the geostrophic forcing, LLJs, and vertical mixing at night were all strong, a nearly neutral boundary layer develops for all test scenarios (Fig. 10e) but the depth of this layer decreases as the mixing weakens. During episode 2, the control run (and also the runs with weaker mixing than in the control run) predicts a strong surface-based inversion, which weakens in the simulations with stronger mixing (Fig. 10f). The coincidence of the heights of LLJ nose and top of the stable

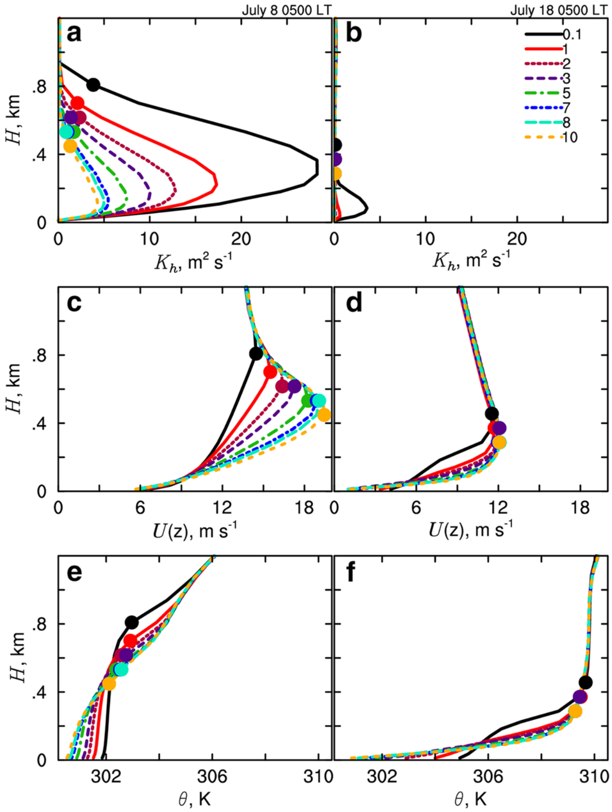

Fig. 10 Vertical profiles of **a**, **b** eddy conductivity K_h, **c**, **d** wind speed $U(z)$, and **e**, **f** potential temperature θ over Oklahoma City at 0500 LT on (*left*) July 8 and (*right*) July 18, 2003 simulated with the WRF model using the YSU PBL scheme with the coefficient a of Eq. 5 varying from 0.1 to 10. The locations of the jet noses are marked with *dots*

boundary layer may be explained by Blackadar's inertial oscillation theory: the oscillation amplitude is expected to grow as the ground is approached from the top of the residual layer until the frictional force inevitably becomes important near the surface in the stable boundary layer (Shapiro and Fedorovich 2010), i.e., the oscillation amplitude at night peaks at the top of the stable boundary layer (Blackadar 1957). The collocation of the LLJ nose and transition from the stable boundary layer to the residual layer also illustrates the importance of nearly zero mixing in the residual layer for the inertial oscillation. These results may also explain why lower LLJs (approximately 100m a.g.l.) are observed in shallower, stably-stratified ocean boundary layers (e.g., Smedman et al. 1995; Mahrt et al. 2014) than in the Southern Great Plains, where the LLJ mostly peaks above 200 m (Song et al. 2005).

Decreasing a in the YSU PBL scheme produces stronger vertical mixing that persists over a deeper layer, leading to higher and weaker LLJs (Fig. 10). Thus, the sensitivity study illustrates how vertical mixing tends to hamper the inertial oscillation and reduce LLJ strength. These results are consistent with the sensitivity tests using analytical models of nocturnal LLJs reported in Shapiro and Fedorovich (2010). In nearly all the quantitative studies of the inertial oscillation using analytical models, turbulent diffusivities or turbu-

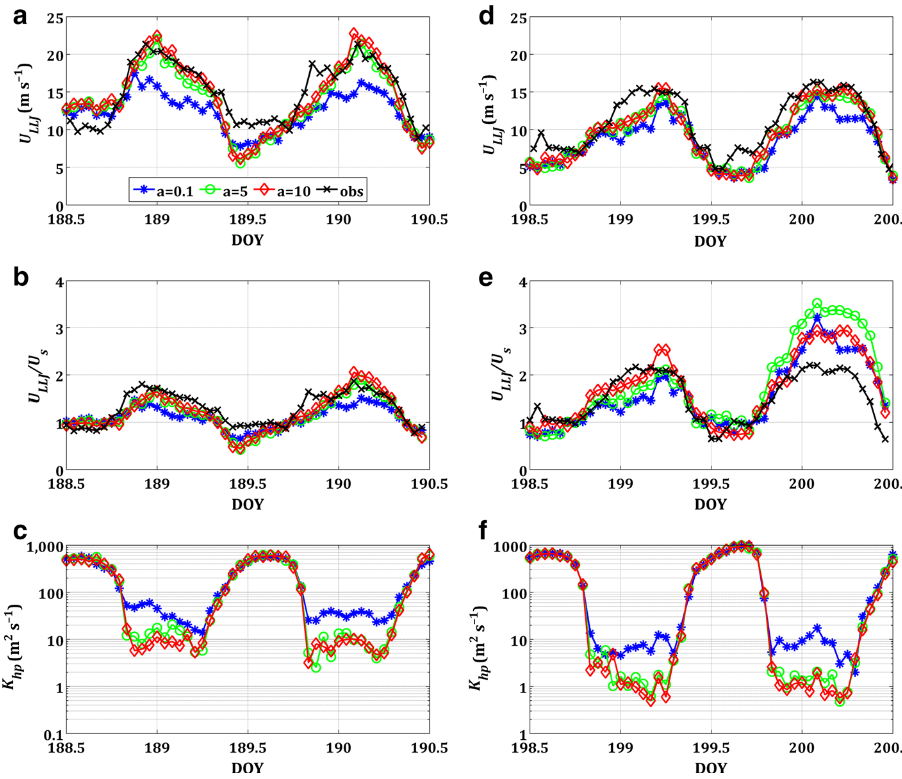

Fig. 11 Time series of **a**, **d** maximum wind speed U_{LLJ}, **b**, **e** relative LLJ strength $U_{\mathrm{LLJ}}/U_{\mathrm{s}}$ and **c**, **f** peak value of the eddy conductivity K_{hp} in the boundary layer during the periods of **a**–**c** July 7–9 (DOY 188–190) and **d**–**f** July 17–19, 2003 (DOY 198–200). Results from WRF model sensitivity tests with the default YSU PBL scheme and three different values of the coefficient a in Eq. 5 are compared against the observations (obs)

lent friction terms were prescribed as external forcings, thus neglecting feedback between the shear and turbulent mixing (Shapiro and Fedorovich 2009, 2010; Van de Wiel et al. 2010; Schroter et al. 2013). This feedback, as shown above, can affect the eventual LLJ strength.

As discussed above, a sharp decrease of vertical mixing in the NBL (including both the stable boundary layer and the residual layer) during the early evening transition can be noted during both episodes (Figs. 9c, d, 11c, f). The simulation results provide additional evidence to the observations that the stronger dynamic forcing during episode 1 caused higher values of U_{LLJ} (Fig. 11a) but weaker relative LLJ strength $U_{\mathrm{LLJ}}/U_{\mathrm{s}}$ (Fig. 11b) than during episode 2 (Fig. 11d, e). Time series (Fig. 11c, f) of the peak values K_{hp} in the vertical eddy-conductivity profiles show that the reduction in K_{hp} during the early evening transition was larger during episode 2 (Fig. 11f) than during episode 1 (Fig. 11c). The fact that $U_{\mathrm{LLJ}}/U_{\mathrm{s}}$ values were higher during episode 2 than during episode 1 confirms that a stronger reduction in vertical turbulent mixing leads to a stronger increase in wind speed after sunset. The results shown in Fig. 12 further illustrate that relative LLJ strength $(U_{\mathrm{LLJ}}/U_{\mathrm{s}})_{\mathrm{night}}$ (maximum value for each night) correlates well with the reduction of eddy conductivity (expressed as the ratio $K_{\mathrm{min}}/K_{\mathrm{max}}$ whereby K_{min} corresponds to the minimum value of K_{hp} observed at night and K_{max} to the maximum of K_{hp} before sunset). The results from both episodes and three different sensitivity

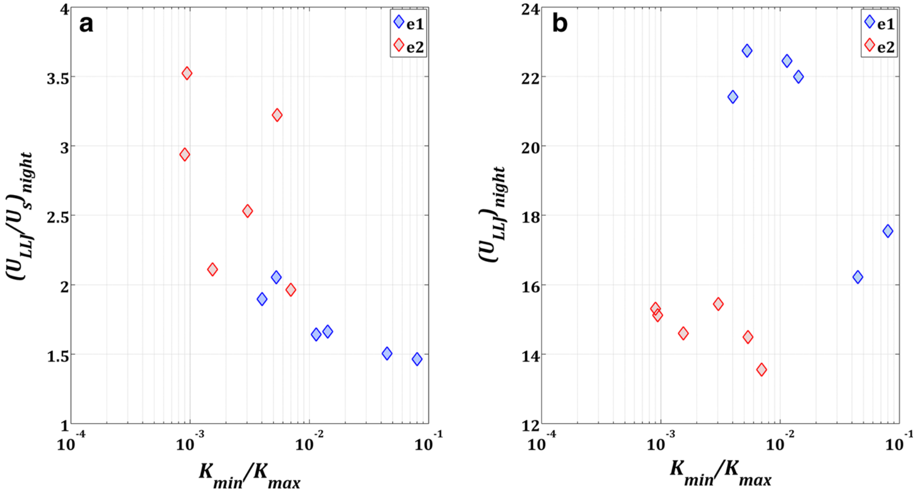

Fig. 12 Variation of **a** relative LLJ strength $(U_{\mathrm{LLJ}}/U_{\mathrm{s}})_{\mathrm{night}}$ and **b** maximum wind speed $(U_{\mathrm{LLJ}})_{\mathrm{night}}$ with the ratio of nighttime to daytime eddy conductivity $K_{\mathrm{min}}/K_{\mathrm{max}}$. The data plotted are based on the WRF model results shown in Fig. 11

tests all show a clear trend of increasing values in relative LLJ strength $(U_{\mathrm{LLJ}}/U_{\mathrm{s}})_{\mathrm{night}}$ as the decrease in turbulent mixing during the early evening transition becomes stronger, i.e., $K_{\mathrm{min}}/K_{\mathrm{max}}$ decreases (Fig. 12a). No clear trends are observed when the actual LLJ speed $(U_{\mathrm{LLJ}})_{\mathrm{night}}$ is plotted against $K_{\mathrm{min}}/K_{\mathrm{max}}$ (Fig. 12b).

In summary, the sensitivity tests conducted with the WRF model have shown that, (1) the numerical simulations are in qualitatively good agreement with observations, (2) the sharp decrease in turbulent mixing during the early evening transition triggers an inertial oscillation, which contributes to LLJ formation, and (3) the scaling of LLJ strength by a scaling velocity U_{s} is critical for investigating the factors leading to LLJ formation. The mixed-layer wind speed, used in our study as scaling velocity U_{s}, overall works well but large differences can be noted between the observations and numerical model results for $U_{\mathrm{LLJ}}/U_{\mathrm{s}}$ on the second day of episode 2 (Fig. 11e). The WRF model predicts much higher values for $U_{\mathrm{LLJ}}/U_{\mathrm{s}}$ than what was observed. These differences can be explained by the underprediction of the afternoon mixed-layer wind speed in the WRF model simulations (Fig. 11d). As a result, the value of the scaling velocity U_{s} from the WRF model was lower than for the observations and consequently $U_{\mathrm{LLJ}}/U_{\mathrm{s}}$ was overpredicted even though the observed and simulated nighttime values of U_{LLJ} agreed well.

4 Discussion and Conclusions

The linkages between LLJ development and properties of the daytime CBL and nighttime stable boundary layer have been investigated by using measurements collected in the Oklahoma City metropolitan area during the Joint Urban 2003 field experiment, along with WRF model simulations. Prominent LLJs occurred on most nights during the JU2003 experiment. According to the inertial oscillation theory (Blackadar 1957), nocturnal LLJs develop in response to the collapse of turbulence in the CBL during the early evening transition. Thus, nights with strong temperature inversions and weak turbulence in a shallow, stable boundary layer near the surface are often viewed as prone to the formation of strong LLJs. Interestingly, the JU2003 datasets show that stronger LLJs in central Oklahoma in the summertime were always associated with stronger turbulence and weaker inversions at night, which could be viewed as contradicting the Blackadar (1957) theory. It is important, though, to find a framework for the data analysis, which allows accounting for the influence of the geostrophic forcing. We have shown that, in the absence of reliable geostrophic winds, the mixed-layer wind speed in the daytime CBL serves as an appropriate LLJ scaling velocity U_{s}. Relative LLJ strength $(U_{\mathrm{LLJ}}/U_{\mathrm{s}})_{\max}$ correlates well with daytime Richardson numbers Ri_{day} and turbulence intensities $(U_{\mathrm{t}}/U_{37})_{\mathrm{day}}$, while the corresponding nighttime values of these two parameters primarily influence the shear below the LLJ nose but do not correlate well with relative LLJ strength.

During nights with stronger LLJs, the wind speeds in the daytime CBL were typically also higher, which indicates that during these days the geostrophic forcing was stronger. As the geostrophic forcing becomes stronger, the rate of mechanically generated turbulence increases both during day and night. It appears that if the wind speed during the early evening transition exceeds a critical value, vertical mixing persists throughout the night and a strong inversion will not develop close to the surface. The development of nocturnal LLJs in the absence of strong surface temperature inversions was also reported in some other regions (e.g., coastal area in high latitudes, Smedman et al. 1995; Helmis et al. 2013). However, even during nights with strong geostrophic forcing, a sharp decrease in vertical mixing is still observed during the early evening transition, which is sufficient to trigger an inertial oscillation. Three-dimensional modelling results further confirm that the sudden weakening of vertical mixing in the NBL (including both the stable boundary layer and the residual layer) during the early evening transition contributes to LLJ formation. The level of mixing at night primarily modulates the thermodynamic structure of the NBL, the height of the LLJ nose and the shear below the jet nose. Stronger/weaker LLJs are associated with stronger/weaker turbulence near the surface, which leads to smaller/greater vertical gradients of temperature and wind speed. These results agree with previous studies (e.g., Lundquist and Mirocha 2008; Hu et al. 2013b, d), which also reported that strong LLJs coincide with strong turbulence near the surface, which modulates the NBL structure.

The NBL characteristics in the presence of LLJs have important implications for vertical dispersion and for the horizontal transport of heat, moisture and pollutants. Under the traditional view of the NBL, the mixing between the surface stable layer and the layer above is limited due to strong stratification. Thus, moisture and pollutants accumulated above the surface layer can be efficiently transported horizontally overnight, especially in the presence of LLJs (Delgado et al. 2014). The present study confirms previous studies (e.g., Banta et al. 2007) that turbulence in a deep NBL can be significant in the presence of strong LLJs. As a result, the vertical distribution of meteorological and chemical variables may be significantly modulated. In the case of ozone, during quiescent nights surface ozone normally decreases through the evening due to dry deposition and chemical reactions. In the presence of strong LLJs, however, strong turbulence plays an important role in transporting ozone-richer residual layer air to the surface leading to nocturnal surface ozone peaks (Hu et al. 2013a; Klein et al. 2014). The impact of LLJs on vertical redistribution and horizontal transport of atmospheric and chemical scalars in the NBL should be further investigated.

The improved understanding of the NBL also has important implications for future model improvement. Model biases for near-surface wind speed, temperature, and pollutants (e.g., ozone) during nighttime are often reported. Systematic over-estimations of near-surface winds during stable conditions have been noted in studies with several meteorological models (e.g., Zhang and Zheng 2004; Miao et al. 2008; Han et al. 2008; Shimada and Ohsawa 2011; Vautard et al. 2012; Garcia-Menendez et al. 2013; Zhang et al. 2013; Wang and Jin 2014).

Such model biases are partially due to inaccurate coupling in the NBL using specific PBL parametrization schemes (Banta et al. 2007; Hu et al. 2013a; Holtslag et al. 2013; Sandu et al. 2013). Several PBL schemes give too strong coupling at night, thus systematically overestimating nighttime near-surface temperature and wind speed (Zhang et al. 2013; Hu et al. 2013a; Ngan et al. 2013). Given the vital importance of PBL schemes for accurate simulations of wind, turbulence, and air quality in the lower atmosphere, evaluation of model simulations with different PBL schemes in terms of their nocturnal coupling, along with the collection of more suitable observations (e.g., vertical profiles of meteorological and chemical variables from Doppler, Raman, and differential absorption lidars), is warranted for providing guidance to future model improvement.

Acknowledgments This work was supported by funding from the Office of the Vice President for Research at the University of Oklahoma. The first author was also supported through the NSF Career award ILREUM (NSF ATM 0547882) and NSF grant AGS-1359698. The fourth author was also supported by NSF grants OCI-0905040, AGS-0802888, AGS-0750790, AGS-0941491, AGS-1046171, and AGS-1046081. WRF model simulations were performed at the Texas Advanced Computing Center.

References

Acevedo OC, Fitzjarrald DR (2001) The early evening surface-layer transition: temporal and spatial variability. J Atmos Sci 58(17):2650–2667. doi:10.1175/1520-0469(2001)0582.0.CO;2

Acevedo OC, Costa FD, Degrazia GA (2012) The coupling state of an idealized stable boundary layer. Boundary-Layer Meteorol 145(1):211–228. doi:10.1007/s10546-011-9676-3

Allwine KJ (2004) Overview of joint urban 2003—an atmospheric dispersion study in Oklahoma City. In: Joint session between the 8th symposium on integrated observing and assimilation systems in the atmosphere, oceans and land surface and the symposium on planning, nowcasting, and forecasting in the urban zone, Seattle, WA. American Meteorological Society

Baas P, Bosveld FC, Baltink HK, Holtslag AAM (2009) A climatology of nocturnal low-level jets at Cabauw. J Appl Meteorol Climatol 48(8):1627–1642. doi:10.1175/2009jamc1965.1

Banta RM (2008) Stable-boundary-layer regimes from the perspective of the low-level jet. Acta Geophys 56(1):58–87. doi:10.2478/s11600-007-0049-8

Banta RM, Newsom RK, Lundquist JK, Pichugina YL, Coulter RL, Mahrt L (2002) Nocturnal low-level jet characteristics over Kansas during CASES-99. Boundary-Layer Meteorol 105(2):221–252. doi:10.1023/a:1019992330866

Banta RM, Pichugina YL, Newsom RK (2003) Relationship between low-level jet properties and turbulence kinetic energy in the nocturnal stable boundary layer. J Atmos Sci 60(20):2549–2555. doi:10.1175/1520-0469(2003)060(aa)2549:rbljpa(aa)2.0.co;2

Banta RM, Pichugina YL, Brewer WA (2006) Turbulent velocity-variance profiles in the stable boundary layer generated by a nocturnal low-level jet. J Atmos Sci 63(11):2700–2719. doi:10.1175/jas3776.1

Banta RM, Mahrt L, Vickers D, Sun J, Balsley BB, Pichugina YL, Williams EL (2007) The very stable boundary layer on nights with weak low-level jets. J Atmos Sci 64:3068–3090. doi:10.1175/jas4002.1

Banta RM, Pichugina YL, Kelley ND, Hardesty RM, Brewer WA (2013) Wind energy meteorology: insight into wind properties in the turbine-rotor layer of the atmosphere from high-resolution Doppler lidar. Bull Am Meteorol Soc 94(6):883–902. doi:10.1175/bams-d-11-00057.1

Belusic D, Guttler I (2010) Can mesoscale models reproduce meandering motions? Q J R Meteorol Soc 136(648):553–565. doi:10.1002/qj.606

Blackadar AK (1957) Boundary layer wind maxima and their significance for the growth of nocturnal inversions. Bull Am Meteorol Soc 38:283–290

Bonin TA, Blumberg WG, Klein PM, Chilson PB (2015) Thermodynamic and kinematic characteristics of the Southern Great Plains nocturnal boundary layer under differing turbulence regimes. Boundary-Layer Meteorol. doi:10.1007/s10546-015-0072-2

Bonner W (1968) Climatology of low level jet. Mon Weather Rev 96(12):833–850. doi:10.1175/1520-0493(1968)096(aa)0833:COTLLJ(aa)2.0.CO;2

Bosveld F, Baas P, Steeneveld G, Holtslag A, Angevine W, Bazile E, de Bruijn E, Deacu D, Edwards J, Ek M, Larson V, Pleim J, Raschendorfer M, Svensson G (2014) The third GABLS intercomparison case for evaluation studies of boundary-layer models. Part B: results and process understanding. Boundary-Layer Meteorol 152(2):157–187. doi:10.1007/s10546-014-9919-1

Chambers S, Williams AG, Zahorowski W, Griffiths A, Crawford J (2011) Separating remote fetch and local mixing influences on vertical radon measurements in the lower atmosphere. Tellus Ser B 63(5):843–859. doi:10.1111/j.1600-0889.2011.00565.x

Chen F, Kusaka H, Bornstein R, Ching J, Grimmond C, Grossman-Clarke S, Loridan T, Manning K, Martilli A, Miao S, Sailor D, Salamanca F, Taha H, Tewari M, Wang X, Wyszogrodzki A, Zhang C (2011) The integrated WRF/urban modelling system: development, evaluation, and applications to urban environmental problems. Int J Climatol 31(2):273–288. doi:10.1002/joc.2158

Conangla L, Cuxart J (2006) On the turbulence in the upper part of the low-level jet: an experimental and numerical study. Boundary-Layer Meteorol 118(2):379–400. doi:10.1007/s10546-005-0608-y

Cuxart J, Jimenez M (2007) Mixing processes in a nocturnal low-level jet: an LES study. J Atmos Sci 64(5):1666–1679. doi:10.1175/JAS3903.1

De Wekker SFJ, Berg LK, Allwine J, Doran JC, Shaw WJ (2004) Boundary-layer structure upwind and downwind of Oklahoma City during the Joint Urban 2003 field study. In: Paper presented at the fifth conference on urban environment, american meteorological society, Vancouver, BC, Canada

Delgado R, Rabenhorst S, Demoz B, Hoff RM (2014) Elastic lidar measurements of summer nocturnal low level jet events over Baltimore, Maryland. J Atmos Chem. doi:10.1007/s10874-013-9277-2

Deppe A, Gallus W, Takle E (2013) A WRF ensemble for improved wind speed forecasts at turbine height. Weather Forecast 28(1):212–228. doi:10.1175/WAF-D-11-00112.1

Draxl C, Hahmann A, Pena A, Giebel G (2014) Evaluating winds and vertical wind shear from Weather Research and Forecasting model forecasts using seven planetary boundary layer schemes. Wind Energy 17(1):39–55. doi:10.1002/we.1555

Duarte H, Leclerc M, Zhang G (2012) Assessing the shear-sheltering theory applied to low-level jets in the nocturnal stable boundary layer. Theor Appl Climatol 110(3):359–371. doi:10.1007/s00704-012-0621-2

Dudhia J (1989) Numerical study of convection observed during the winter monsoon experiment using a mesoscale 2-dimenional model. J Atmos Sci 46(20):3077–3107. doi:10.1175/1520-0469(1989)046(aa)3077:NSOCOD(aa)2.0.CO;2

Edwards J, Basu S, Bosveld F, Holtslag A (2014) The impact of iadiation on the GABLS3 large-eddy simulation through the night and during the morning transition. Boundary-Layer Meteorol 152(2):189–211. doi:10.1007/s10546-013-9895-x

Fast J, McCorcle M (1990) A 2-dimensional numerical sensitivity study of the Great-Plains low-level jet. Mon Weather Rev 118(1):151–163. doi:10.1175/1520-0493(1990)118(aa)0151:ATDNSS(aa)2.0.CO;2

Fernando HJS, Weil JC (2010) Whither the stable boundary layer? A shift in the research agenda. Bull Am Meteorol Soc 91(11):1475–1484. doi:10.1175/2010bams2770.1

Fiebrich CA, Crawford KC (2001) The impact of unique meteorological phenomena detected by the Oklahoma Mesonet and ARS Micronet on automated quality control. Bull Am Meteorol Soc 82(10):2173–2187. doi:10.1175/1520-0477(2001)0822.3.CO;2

Foken T (2006) 50 years of the Monin–Obukhov similarity theory. Bound-Layer Meteorol 119(3):431–447. doi:10.1007/s10546-006-9048-6

Garcia-Menendez F, Hu Y, Odman M (2013) Simulating smoke transport from wildland fires with a regional-scale air quality model: sensitivity to uncertain wind fields. J Geophys Res 118(12):6493–6504. doi:10.1002/jgrd.50524

Grimmond CSB, Su H-B, Offerle B, Crawford B, Scott S, Zhong S, Clements C (2004) Variability of sensible heat fluxes in a suburban area of Oklahoma City. In: Paper presented at the symposium on planning, nowcasting, and forecasting in the urban zone/eighth symposium on integrated observing and assimilation systems for atmosphere, oceans, and land surface, Seattle, WA, USA

Ha K, Mahrt L (2001) Simple inclusion of z-less turbulence within and above the modeled nocturnal boundary layer. Mon Weather Rev 129(8):2136–2143. doi:10.1175/1520-0493(2001)129(aa)2136:SIOZLT(aa)2.0.CO;2

Han Z, Ueda H, An J (2008) Evaluation and intercomparison of meteorological predictions by five MM5-PBL parameterizations in combination with three land-surface models. Atmos Environ 42(2):233–249. doi:10.1016/j.atmosenv.2007.09.053

Helmis C, Wang Q, Sgouros G, Wang S, Halios C (2013) Investigating the summertime low-level jet over the east coast of the USA: a case study. Boundary-Layer Meteorol 149(2):259–276. doi:10.1007/s10546-013-9841-y

Holton JR (1967) The diurnal boundary layer wind oscillation above sloping terrain. Tellus 19:199–205. doi:10.1111/j.2153-3490.1967.tb01473.x

Holtslag AAM, Svensson G, Baas P, Basu S, Beare B, Beljaars ACM, Bosveld FC, Cuxart J, Lindvall J, Steeneveld GJ, Tjernstrom M, Van de Wiel BJH (2013) Stable atmospheric boundary layers and diurnal cycles—challenges for weather and climate models. Bull Am Meteorol Soc 94(11):1691–1706. doi:10.1175/bams-d-11-00187.1

Hong S-Y (2010) A new stable boundary-layer mixing scheme and its impact on the simulated East Asian summer monsoon. Q J R Meteorol Soc 136(651):1481–1496. doi:10.1002/qj.665

Hong SY, Dudhia J, Chen SH (2004) A revised approach to ice microphysical processes for the bulk parameterization of clouds and precipitation. Mon Weather Rev 132(1):103–120. doi:10.1175/1520-0493(2004)132(aa)0103:aratim(aa)2.0.co;2

Hong S-Y, Noh Y, Dudhia J (2006) A new vertical diffusion package with an explicit treatment of entrainment processes. Mon Weather Rev 134(9):2318–2341. doi:10.1175/mwr3199.1

Hu X-M, Doughty DC, Sanchez KJ, Joseph E, Fuentes JD (2012) Ozone variability in the atmospheric boundary layer in Maryland and its implications for vertical transport model. Atmos Environ 46:354–364. doi:10.1016/j.atmosenv.2011.09.054

Hu X-M, Klein PM, Xue M (2013a) Evaluation of the updated YSU planetary boundary layer scheme within WRF for wind resource and air quality assessments. J Geophys Res 118(18):10490–10505. doi:10.1002/jgrd.50823

Hu X-M, Klein PM, Xue M, Lundquist JK, Zhang F, Qi Y (2013b) Impact of low-level jets on the nocturnal urban heat island intensity in Oklahoma City. J Appl Meteorol Climatol 52(8):1779–1802. doi:10.1175/jamc-d-12-0256.1

Hu X-M, Klein PM, Xue M, Shapiro A, Nallapareddy A (2013c) Enhanced vertical mixing associated with a nocturnal cold front passage and its impact on near-surface temperature and ozone concentration. J Geophys Res 118(7):2714–2728. doi:10.1002/jgrd.50309

Hu X-M, Klein PM, Xue M, Zhang F, Doughty DC, Forkel R, Joseph E, Fuentes JD (2013d) Impact of the vertical mixing induced by low-level jets on boundary layer ozone concentration. Atmos Environ 70:123–130. doi:10.1016/j.atmosenv.2012.12.046

Jiang X, Lau N-C, Held IM, Ploshay JJ (2007) Mechanisms of the great plains low-level jet as simulated in an AGCM. J Atmos Sci 64(2):532–547. doi:10.1175/jas3847.1

Kallistratova M, Kouznetsov R, Kuznetsov D, Kuznetsova I, Nakhaev M, Chirokova G (2009) Summertime low-level jet characteristics measured by sodars over rural and urban areas. Meteorol Z 18(3):289–295. doi:10.1127/0941-2948/2009/0380

Karipot A, Leclerc MY, Zhang G, Lewin KF, Nagy J, Hendrey GR, Starr G (2008) Influence of nocturnal low-level jet on turbulence structure and CO2 flux measurements over a forest canopy. J Geophys Res. doi:10.1029/2007jd009149

Klein P, Bonin TA, Newman JF, Turner DD, Chilson PB, Wainwright CE, Blumberg WG, Mishra S, Carney M, Jacobsen EP, Wharton S, Newsom RK (2015) LABLE: a multi-institutional, student-led, atmospheric boundary-layer experiment. Bull Am Meteorol Soc. doi:10.1175/BAMS-D-13-00267.1

Klein PM, Hu X-M, Xue M (2014) Impacts of mixing processes in nocturnal atmospheric boundary layer on urban ozone concentrations. Boundary-Layer Meteorol 150(1):107–130. doi:10.1007/s10546-013-9864-4

Kutsher J, Haikin N, Sharon A, Heifetz E (2012) On the formation of an elevated nocturnal inversion layer in the presence of a low-level jet: a case study. Boundary-Layer Meteorol 144(3):441–449. doi:10.1007/s10546-012-9720-y

Lareau N, Crosman E, Whiteman C, Horel J, Hoch S, Brown W, Horst T (2013) The persistent cold-air pool study. Bull Am Meteorol Soc 94(1):51–63. doi:10.1175/BAMS-D-11-00255.1

Lemonsu A, Belair S, Mailhot J (2009) The new Canadian urban modelling system: Evaluation for two cases from the Joint Urban 2003 Oklahoma City Experiment. Boundary-Layer Meteorol 133(1):47–70. doi:10.1007/s10546-009-9414-2

Liu Y, Chen F, Warner T, Basara J (2006) Verification of a mesoscale data-assimilation and forecasting system for the Oklahoma City area during the Joint Urban 2003 field project. J Appl Meteorol Climatol 45(7):912–929. doi:10.1175/JAM2383.1

Lundquist J (2003) Intermittent and elliptical inertial oscillations in the atmospheric boundary layer. J Atmos Sci 60(21):2661–2673. doi:10.1175/1520-0469(2003)060(aa)2661:IAEIOI(aa)2.0.CO;2

Lundquist J, Mirocha J (2008) Interaction of nocturnal low-level jets with urban geometries as seen in joint urban 2003 data. J Appl Meteorol Climatol 47(1):44–58. doi:10.1175/2007JAMC1581.1

Mahrt L (1999) Stratified atmospheric boundary layers. Boundary-Layer Meteorol 90(3):375–396. doi:10.1023/a:1001765727956

Mahrt L (2007) Weak-wind mesoscale meandering in the nocturnal boundary layer. Environ Fluid Mech 7(4):331–347. doi:10.1007/s10652-007-9024-9

Mahrt L (2009) Characteristics of submeso winds in the stable boundary layer. Boundary-Layer Meteorol 130(1):1–14. doi:10.1007/s10546-008-9336-4

Mahrt L (2010) Variability and maintenance of turbulence in the very stable boundary Layer. Boundary-Layer Meteorol 135(1):1–18. doi:10.1007/s10546-009-9463-6

Mahrt L (2011) Surface wind direction variability. J Appl Meteorol Climatol 50(1):144–152. doi:10.1175/2010jamc2560.1

Mahrt L (2014) Stably stratified atmospheric boundary layers. Annu Rev Fluid Mech 46(46):23–45. doi:10.1146/annurev-fluid-010313-141354

Mahrt L, Vickers D (2002) Contrasting vertical structures of nocturnal boundary layers. Boundary-Layer Meteorol 105(2):351–363. doi:10.1023/a:1019964720989

Mahrt L, Vickers D, Andreas EL (2014) Low-level wind maxima and structure of the stably stratified boundary layer in the coastal zone. J Appl Meteorol Climatol 53(2):363–376. doi:10.1175/jamc-d-13-0170.1

McPherson RA, Fiebrich CA, Crawford KC, Elliott RL, Kilby JR, Grimsley DL, Martinez JE, Basara JB, Illston BG, Morris DA, Kloesel KA, Stadler SJ, Melvin AD, Sutherland AJ, Shrivastava H, Carlson JD, Wolfinbarger JM, Bostic JP, Demko DB (2007) Statewide monitoring of the mesoscale environment: a technical update on the Oklahoma Mesonet. J Atmos Ocean Technol 24(3):301–321. doi:10.1175/jtech1976.1

Miao JF, Chen D, Wyser K, Borne K, Lindgren J, Strandevall MKS, Thorsson S, Achberger C, Almkvist E (2008) Evaluation of MM5 mesoscale model at local scale for air quality applications over the Swedish west coast: Influence of PBL and LSM parameterizations. Meteorol Atmos Phys 99(1–2):77–103. doi:10.1007/s00703-007-0267-2

Mitchell MJ, Arritt RW, Labas K (1995) A climatology of the warm-season Great-Plains low-level jet using wind profiler observations. Weather Forecast 10(3):576–591. doi:10.1175/1520-0434(1995)010(aa)0576:acotws(aa)2.0.co;2

Mlawer EJ, Taubman SJ, Brown PD, Iacono MJ, Clough SA (1997) Radiative transfer for inhomogeneous atmospheres: RRTM, a validated correlated-k model for the longwave. J Geophys Res 102(D14):16663–16682. doi:10.1029/97jd00237

Ngan F, Kim H, Lee P, Al-Wali K, Dornblaser B (2013) A Study of nocturnal surface wind speed overprediction by the WRF-ARW Model in southeastern Texas. J Appl Meteorol Climatol 52(12):2638–2653. doi:10.1175/JAMC-D-13-060.1

Nielsen-Gammon J, Hu X, Zhang F, Pleim J (2010) Evaluation of planetary boundary layer scheme sensitivities for the purpose of parameter estimation. Mon Weather Rev 138(9):3400–3417. doi:10.1175/2010MWR3292.1

Ohya Y, Nakamura R, Uchida T (2008) Intermittent bursting of turbulence in a stable boundary layer with low-level jet. Bound-Layer Meteorol 126(3):349–363. doi:10.1007/s10546-007-9245-y

Pan Z, Segal M, Arritt R (2004) Role of topography in forcing low-level jets in the Central United States during the 1993 flood-altered terrain simulations. Mon Weather Rev 132(1):396–403. doi:10.1175/1520-0493(2004)132(aa)0396:ROTIFL(aa)2.0.CO;2

Parish T, Oolman L (2010) On the role of sloping terrain in the forcing of the Great Plains low-level jet. J Atmos Sci 67(8):2690–2699. doi:10.1175/2010JAS3368.1

Pichugina Y, Banta R (2010) Stable boundary layer depth from high-resolution measurements of the mean wind profile. J Appl Meteorol Climatol 49(1):20–35. doi:10.1175/2009JAMC2168.1

Pu B, Dickinson R (2014) Diurnal spatial variability of Great Plains summer precipitation related to the dynamics of the low-level jet. J Atmos Sci 71(5):1807–1817. doi:10.1175/JAS-D-13-0243.1

Sandu I, Beljaars A, Bechtold P, Mauritsen T, Balsamo G (2013) Why is it so difficult to represent stably stratified conditions in numerical weather prediction (NWP) models? J Adv Model Earth Syst 5(2):117–133. doi:10.1002/jame.20013

Schroter J, Moene A, Holtslag A (2013) Convective boundary layer wind dynamics and inertial oscillations: the influence of surface stress. Q J R Meteorol Soc 139(676):1694–1711. doi:10.1002/qj.2069

Shapiro A, Fedorovich E (2009) Nocturnal low-level jet over a shallow slope. Acta Geophys 57(4):950–980. doi:10.2478/s11600-009-0026-5

Shapiro A, Fedorovich E (2010) Analytical description of a nocturnal low-level jet. Q J R Meteorol Soc 136(650):1255–1262. doi:10.1002/qj.628

Shibuya R, Sato K, Nakanishi M (2014) Diurnal wind cycles forcing inertial oscillations: a latitude-dependent resonance phenomenon. J Atmos Sci 71(2):767–781. doi:10.1175/jas-d-13-0124.1

Shimada S, Ohsawa T (2011) Accuracy and characteristics of offshore wind speeds simulated by WRF. Sola 7:21–24. doi:10.2151/sola.2011-006

Shin H, Hong S (2011) Intercomparison of planetary boundary-layer parametrizations in the WRF model for a single day from CASES-99. Boundary-Layer Meteorol 139(2):261–281. doi:10.1007/s10546-010-9583-z

Skamarock WC, Klemp JB, Dudhia J, Gill DO, Barker DM, Duda MG, Huang XY, Wang W, Powers JG (2008) A Description of the advanced research WRF Version 3. NCAR Technical Note. National Center for Atmospheric Research Boulder, CO, USA
Smedman A, Bergstrom H, Hogstrom U (1995) Spectra, variances and length scales in a marine stable boundary layer dominated by a low level jet. Boundary-Layer Meteorol 76(3):211–232. doi:10.1007/BF00709352
Smedman A, Bergstrom H, Grisogono B (1997) Evolution of stable internal boundary layers over a cold sea. J Geophys Res 102(C1):1091–1099. doi:10.1029/96JC02782
Song J, Liao K, Coulter R, Lesht B (2005) Climatology of the low-level jet at the southern Great Plains atmospheric boundary layer experiments site. J Appl Meteorol 44(10):1593–1606. doi:10.1175/JAM2294.1
Stensrud D (1996) Importance of low-level jets to climate: a review. J Clim 9(8):1698–1711. doi:10.1175/1520-0442(1996)009(aa)1698:IOLLJT(aa)2.0.CO;2
Storm B, Dudhia J, Basu S, Swift A, Giammanco I (2009) Evaluation of the Weather Research and Forecasting model on forecasting low-level jets: implications for wind energy. Wind Energy 12(1):81–90. doi:10.1002/we.288
Sun J, Mahrt L, Banta R, Pichugina Y (2012) Turbulence regimes and turbulence intermittency in the stable boundary layer during CASES-99. J Atmos Sci 69(1):338–351. doi:10.1175/JAS-D-11-082.1
Van de Wiel B, Moene A, Steeneveld G, Baas P, Bosveld F, Holtslag A (2010) A conceptual view on inertial oscillations and nocturnal low-level jets. J Atmos Sci 67(8):2679–2689. doi:10.1175/2010JAS3289.1
Van de Wiel B, Moene A, Jonker H (2012a) The cessation of continuous turbulence as precursor of the very stable nocturnal boundary layer. J Atmos Sci 69(11):3097–3115. doi:10.1175/JAS-D-12-064.1
Van de Wiel B, Moene A, Jonker H, Baas P, Basu S, Donda J, Sun J, Holtslag A (2012b) The minimum wind speed for sustainable turbulence in the nocturnal boundary layer. J Atmos Sci 69(11):3116–3127. doi:10.1175/JAS-D-12-0107.1
Vautard R, Moran M, Solazzo E, Gilliam R, Matthias V, Bianconi R, Chemel C, Ferreira J, Geyer B, Hansen A, Jericevic A, Prank M, Segers A, Silver J, Werhahn J, Wolke R, Rao S, Galmarini S (2012) Evaluation of the meteorological forcing used for the Air Quality Model Evaluation International Initiative (AQMEII) air quality simulations. Atmos Environ 53:15–37. doi:10.1016/j.atmosenv.2011.10.065
Wang C, Jin S (2014) Error features and their possible causes in simulated low-level winds by WRF at a wind farm. Wind Energy 17(9):1315–1325. doi:10.1002/we.1635
Wang Y, Klipp CL, Garvey DM, Ligon DA, Williamson CC, Chang SS, Newsom RK, Calhoun R (2007) Nocturnal low-level-jet-dominated atmospheric boundary layer observed by a Doppler lidar over Oklahoma City during JU2003. J Appl Meteorol Climatol 46(12):2098–2109. doi:10.1175/2006jamc1283.1
Wei W, Wu B, Ye X, Wang H, Zhang H (2013) Characteristics and mechanisms of low-level jets in the Yangtze River delta of China. Boundary-Layer Meteorol 149(3):403–424. doi:10.1007/s10546-013-9852-8
Wei W, Zhang H, Ye X (2014) Comparison of low-level jets along the north coast of China in summer. J Geophys Res 119(16):9692–9706. doi:10.1002/2014JD021476
Werth D, Kurzeja R, Dias N, Zhang G, Duarte H, Fischer M, Parker M, Leclerc M (2011) The simulation of the Southern Great Plains nocturnal boundary layer and the low-level jet with a high-resolution mesoscale atmospheric model. J Appl Meteorol Climatol 50(7):1497–1513. doi:10.1175/2011JAMC2272.1
Wexler H (1961) A boundary layer interpretation of the low-level jet. Tellus 13(3):368–378
Williams A, Chambers S, Griffiths A (2013) Bulk mixing and decoupling of the nocturnal stable boundary layer characterized using a ubiquitous natural tracer. Boundary-Layer Meteorol 149(3):381–402. doi:10.1007/s10546-013-9849-3
Zhang D, Zheng W (2004) Diurnal cycles of surface winds and temperatures as simulated by five boundary layer parameterizations. J Appl Meteorol 43(1):157–169. doi:10.1175/1520-0450(2004)043(aa)0157:DCOSWA(aa)2.0.CO;2
Zhang D, Zhang S, Weaver S (2006) Low-level jets over the Mid-Atlantic states: warm-season climatology and a case study. J Appl Meteorol Climatol 45(1):194–209. doi:10.1175/JAM2313.1
Zhang H, Pu Z, Zhang X (2013) Examination of errors in near-surface temperature and wind from WRF numerical simulations in regions of complex terrain. Weather Forecast 28(3):893–914. doi:10.1175/WAF-D-12-00109.1
Zhong S, Fast J, Bian X (1996) A case study of the great plains low-level jet using wind profiler network data and a high-resolution mesoscale model. Mon Weather Rev 124(5):785–806. doi:10.1175/1520-0493(1996)124(aa)0785:ACSOTG(aa)2.0.CO;2